



UNIVERSITY
OF TRENTO - Italy

DEPARTMENT OF INDUSTRIAL ENGINEERING

XXVII cycle

Doctoral School in Materials Science and Engineering

***Synthesis and Characterization of
Calcium Phosphate Powders for
Biomedical Applications by Plasma
Spray Coating***

Sasidharan Pillai Rahul

Advisor: Prof. Vincenzo. M. Sglavo

April – 2015

***Synthesis and Characterization of Calcium
Phosphate Powders for Biomedical Applications
by Plasma Spray Coating***

Rahul Sasidharan Pillai

E-mail: r.sasidharanpillai@unitn.it

Approved by:

Prof. Vincenzo M. Sglavo,
Advisor
Department of Industrial Engineering
University of Trento, Italy
vincenzo.sglavo@unitn.it

Ph.D. Commission:

Prof. Gian Domenico Soraru,
Department of Industrial Engineering
University of Trento, Italy.

Prof. Ralf Riedel,
Fachbereich Material- und
Geowissenschaften
Technical University Darmstadt,
Darmstadt, Germany.

Prof. Sabine Fuchs,
Department of Traumatology
Experimental Trauma Surgery
University Hospital Schleswig-
Holstein, Campus Kiel, Germany.

University of Trento,
Department of Industrial Engineering

April 2015

University of Trento - Department of Industrial Engineering

Doctoral Thesis

Rahul Sasidharan Pillai - 2015

Published in Trento (Italy) – by University of Trento

ISBN:

To My Teachers

Table of Contents

Thesis Overview.....	7
Chapter 1: Introduction	11
1.1. Orthopaedic implants	14
1.2. Bioceramics.....	15
1.3. Biodegradable or resorbable ceramics.....	16
1.4. Calcium Phosphate (CaP).....	17
1.5. Hydroxyapatite	20
1.6. Beta tricalcium phosphate (β TCP).....	24
1.7. Doping of β TCP	27
1.8. Plasma Spray Coatings.....	29
Chapter 2: Materials and Methods	32
2.1. Solid state synthesis method.....	32
2.1.1. MgO-doped β TCP powder	32
2.1.2. HA/ β TCP (60:40) composite powders	33
2.2. Invitro analysis.....	38
2.2.1. Bioactivity behaviour	38
2.2.2. Solubility Measurements.....	40
Chapter 3: Results and Discussions	41
3.1. Solid state Synthesis	41

3.1.1. MgO doped β TCP powder	41
3.1.2. HA/ β TCP composite powders.....	54
3.1.8. Invitro studies of TCP coatings	83
Chapter 4: Conclusion	90
Reference:	92
Acknowledgements	103
Curriculum Vitae	105
Publications	106
Conferences	108

Thesis Overview

The excellent biocompatibility and osteointegration properties of calcium phosphate-based materials in different forms ranging from dense to porous bodies or as granules and coatings is well utilised in dental and skeletal prosthetic applications. Hydroxyapatite (HA- $\text{Ca}_5(\text{PO}_4)_3(\text{OH})$) and beta tricalcium phosphate (βTCP , $\beta\text{-Ca}_3(\text{PO}_4)_3$) are typically used compositions in biomedical applications due to their chemical similarity to the inorganic component of human bone and teeth. It is to be noted that human hard tissues are not pure HA or βTCP and it contain other organic compounds (collagen and non - collagenous proteins) and inorganic phosphates as well, which are isomorphically substituted by several ions like Mg^{2+} , Sr^{2+} , Na^+ , K^+ etc. in trace level. It is now well known that the presence of such trace elements plays an essential role in biological metabolism, and their introduction in synthetic biomaterials can modify and even improve the biocompatibility and osteointegration process.

The raw materials used for hard tissue bioengineering applications are typically calcium phosphate ceramic powders. Different production methods, including solid-state, hydro-thermal and wet chemical processes have been developed for their synthesis. Among these approaches, solid-state route is preferred mainly because of its simplicity and lower number of controlling parameters. Other techniques require obeying several strict

processing conditions like reaction temperature, time and solution pH; a slight variation of any of these conditions can cause the formation of other phosphate phases, which are undesirable.

This PhD work mainly focus on the synthesis and characterization of calcium phosphate powders for plasma spray coating. The preparation of high temperature phase stabilized β TCP and HA/ β TCP powders for plasma spray coating applications has been the topic of investigation. Nowadays plasma sprayed coatings are widely used for biomedical applications especially in the dental and orthopaedic implantation field. Previously Ti based alloys were widely used for the orthopaedic and dental implant applications because of its high corrosion and good biocompatibility. Due to the limited osteoconductivity edges of Ti implants with fibrous tissues delays the healing time. To overcome these limitations different types of surface modification processes are employed on the surface of Ti. The coating of HA is a widely used surface modification technique due to its excellent biological properties. HA is a well employed bone graft material due to its similarity with human hard tissues. The plasma spraying of HA on the Ti surface is the most widely used technique mainly due to its process simplicity, low cost and bulk production.

The present research focuses on the modification of HA coatings for the improvement of bio-degradation properties of HA. HA/ β TCP composite powders are used to overcome the poor biodegradation properties of HA.

The issue related to the use of β TCP is the phase transformation (β to α) at high temperature. To overcome this phase transformation, the β TCP powder was doped with MgO. The high temperature phase stabilized MgO doped β TCP and HA/ β TCP powders were synthesized by solid state method and granulated using spray granulation. The properties of the granulated powders (100-150 μ m) were analysed with XRD, FT-IR, SEM, flowability, density etc. and are used in plasma spray coating process. The produced coatings were subjected to the thermal treatment and β TCP and HA/ β TCP plasma sprayed coatings are obtained. The successively produced coatings were characterized, and the invitro properties like solubility and bioactivity behaviours were studied.

Chapter 1: Introduction

The end of the 19th century witnessed the introduction of the concept of aseptic surgery, and its further development led to the possibility of implanting foreign material into the human body with an acceptably low risk of rejection due to infections. Nevertheless, at this time no suitable material was existing, which could withstand the challenges caused by the biological environment. Later on, in the first half of 20th century improved materials were developed and were used in the surgical applications. The materials currently in use are those that have performed tolerably in clinical situations. *Inter alia*, the developments in the field of biomaterial research over the past 20 years had a great influence on the technologic advances in this regard. A biomaterial is any matter, surface or construct that interacts with human biological systems. In the present epoch, the biomaterial science is a well-developed and expanded area of research and a huge amount of money is invested by industry for the development of biomaterials. Also biomaterial research has become an interdisciplinary area comprising almost all areas of scientific research including medicine, biology, chemistry, tissue engineering and material science.

A biomaterial can communicate with human tissues and body fluids to improve or replace the morphology and structure of a human body. Over the past few decades, the advent of artificial implantation has ushered

several advances in the biomedical field. Biomaterials can be derived either from nature or can be produced in the laboratory using different chemical approaches involving metallic and non metallic components, polymers, ceramics and composite materials. Nowadays, biomaterials are widely used in joint replacement, bone plates, bone cement, artificial ligaments, tendons, dental implants, blood vessel prostheses and heart valves. Also they find application in skin repair devices (artificial tissue), cochlear replacements, contact lenses, breast implants, drug delivery mechanisms, sustainable materials, vascular grafts, and nerve conduits. **Figure 1** shows the applications of biomaterials in the human body.

Biocompatibility plays an important role in the application of biomaterial products, because it must be adaptable in human body and should not be rejected by the human immune system. Due to the high demand for synthetic biomaterials to assist and replace skeletal tissue, and the high failure rates of these medical implants, a great deal of research focuses on improving the strength of implant tissue interface and in the design of implants that degrade in concert with the natural healing process. Artificial soft tissues and organs are the products of the recent bio-medical research. The artificial materials are synthesized mainly from bio active materials with similar properties of human soft and hard tissues. Research on the development of new biomaterials includes the use of the present materials in a new composite material with enhanced properties,

modification of the structure of the present biomaterials and the chemical synthesis of new biomaterials. [1, 2]

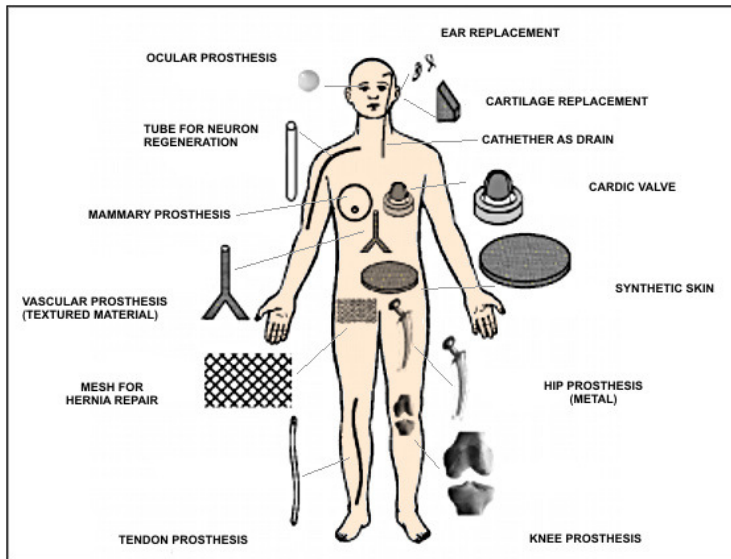


Figure 1: Applications of biomaterials in the human body an over view [81]

Particularly, orthopaedic implants constitute a major part in the biomedical implantation. The increase in the implants percentage boosts more exploration in this area.

1.1. Orthopaedic implants

Orthopaedic implants can be defined as medical devices used to replace or provide fixation of bone, or articulating surface of a joint. The final success and life time of orthopaedic implants are determined by the bone-implant reaction with human body or tissue. Nowadays orthopaedic implants are available for hip, knee, shoulder and elbow.

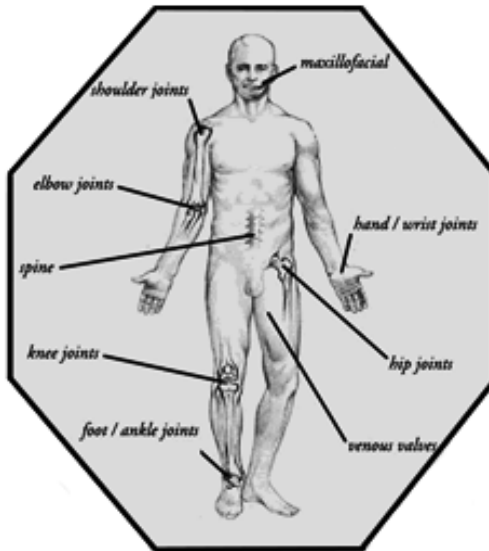


Figure 2: Applications of orthopedic implants in the human body

(Source: <http://www.onxlti.com/product-divisions/contract-manufacturing-products/orthopedic-applications/>)

Till date, the best available materials for orthopaedic implants are titanium and calcium phosphate ceramics. [3,4]

1.2. Bioceramics

<i>Type of Bioceramics</i>	<i>Properties</i>	<i>Example</i>
Non absorbable (relatively inert)	Attach by bone growth into surface irregularities by cementing the device in to the tissues or by press fitting into a defect (morphological fixation)	Al ₂ O ₃ , Zirconia, Silicon nitrides and carbons
Bioactive and surface reactive (semi inert)	Direct chemical bond with bone. (Bioactive fixation)	Dense hydroxyapatite and glass ceramics
Biodegradable or resorbable	Slowly replaced by bone	Tricalcium phosphate, Calcium phosphate salts and Calcium sulphate (plaster of paris)

Table 1: Different types of bioceramics and its properties [5].

A ceramic is an inorganic non metallic solid prepared by the action of heat with consecutive cooling. Mostly, they have crystalline nature and some of them are amorphous. In the recent years, we have realized that ceramics and their composites can also be used to augment or replace various parts of the human body, especially hard body parts like bone and teeth, because of its biocompatibility nature and structural properties. The ceramics which are used in the biomedical applications are called bio-ceramics. The main advantage of bio-ceramics is its high compatibility with human body environment and the fact that it contains ions, which are commonly found in the body tissues. The advantage of the ceramic material is the comparatively faster bond formation between the tissue and the material. Bioceramics are classified into four groups based on the types of attachment to the surrounding tissues. **Table 1** shows the different types of bioceramics, properties and examples. [5] [6]

1.3. Biodegradable or resorbable ceramics

Resorbable ceramics, as the name implies, degrade upon implantation in the body. The rate of degradation varies with the property of the implanting material. Tricalcium phosphate, plaster of paris, hydroxyapatite, corallines, *etc.* are the examples of easily available resorbable biomaterials. Implantation failures due to infection and other biological issues with

human body are well surpassed by calcium phosphate because of its excellent properties comparable with human soft and hard tissues. [5]

1.4. Calcium Phosphate (CaP)

The excellent biocompatibility and osteointegration properties of calcium phosphate based materials in different forms ranging from dense to porous bodies or granules and coating is well utilised in dental and skeletal prosthetic applications. The surface reactivity of calcium phosphate based materials contribute to the bone bonding ability and increased the new bone tissue formation. Also these materials are non toxic and they will not cause the death of surrounding tissues. The main advantage of calcium phosphate is that, it is already present in the human body in different biological systems. **Table 2** shows the different types of calcium phosphates in the human biological system.

<i>Calcium phosphates</i>	<i>Occurrence</i>
Amorphous calcium phosphates (ACP)	Soft- tissue calcification
Dicalcium phosphate dihydrate (DCPD)	Dental calculus, dental caries
Octacalcium phosphate (OCP)	Dental calculus, urinary stone
Mg-substituted tricalcium phosphate (β TCMP)	Dental calculus, soft tissue calcification
Carbonate hydroxyapatite (CHA)	Dental calculus, urinary stone, mineral phase of enamel, dentin, cementum, bone, fish enameloids
Carbonate fluoroapatite (CFA), Calcium pyrophosphate dihydrate (CPPD)	Fish enameloids

Table 2: Applications of calcium phosphate in biological systems [77]

The main advantages of calcium phosphate in biomedical applications are

- 1) The ability for the formation of new bone apatite like minerals on the surface.
- 2) The structural similarity and phase composition with human hard tissue minerals.
- 3) The ability of releasing Ca and phosphorous ions and the solubility which boosts the cellular function and new bone formation.

- 4) The resorbability property of calcium phosphate which helps the formation and reabsorption occurring in the bone tissue.

The raw materials for bioengineering applications are typically calcium phosphate ceramic powders. The utilisation of synthetic calcium phosphates in multi functional biomedical applications such as orthopaedic, aesthetic, healing bone defects, bio imaging etc was a major breakthrough in recent years. Calcium phosphates are categorised depending up on the chemical composition with respect to the Ca/P molar ratio and solubility. Commonly calcium phosphates containing lower Ca/P ratio are more acidic and hence more soluble in body fluids.

Compound	Formula	Ca/P ratio	Solubility at 25°C
Monocalcium phosphate monohydrate (MCPM)	$\text{Ca}(\text{H}_2\text{PO}_4)_2 \cdot \text{H}_2\text{O}$	0.5	1.14
Monocalcium phosphate anhydrous (MCPA)	$\text{Ca}(\text{H}_2\text{PO}_4)_2$	0.5	1.14
Dicalcium phosphate dihydrate (DCPD)	$\text{CaHPO}_4 \cdot 2\text{H}_2\text{O}$	1.0	6.59
Dicalcium phosphate anhydrous (DCP)	CaHPO_4	1.0	6.90
Octacalcium phosphate (OCP)	$\text{Ca}_8\text{H}_2(\text{PO}_4)_6 \cdot 5 \text{H}_2\text{O}$	1.33	96.6
α -tricalcium phosphate (α -TCP)	$\alpha\text{-Ca}_3(\text{PO}_4)_2$	1.5	25.5
β -tricalcium phosphate (β -TCP)	$\beta\text{-Ca}_3(\text{PO}_4)_2$	1.5	2.5
Hydroxyapatite (HA)	$\text{Ca}_{10}(\text{PO}_4)_6(\text{OH})_2$	1.67	116.8
Tetracalcium phosphate (TTCP)	$\text{Ca}_4(\text{PO}_4)_2$	2.0	38-44

Table 3: Existing calcium phosphate and their major properties[78,79]

Calcium phosphate can be divided into different compounds depending on the chemical compositions associated to the molar Ca/P ratio and solubility. In general as lower the ratio Ca/P is more acidic and more soluble become in the water. Hydroxyapatite (HA) and β -tricalcium phosphate (β TCP) are the most stable and least soluble calcium phosphate from the group (**table 3**) because of this nature they are commonly used for biomedical applications.

1.5. Hydroxyapatite

Over the past years, hydroxyapatite (hydroxylapatite- $\text{Ca}_{10}((\text{PO}_4)_6(\text{OH})_2)$) received much attention as a replacing material for damaged bone and teeth in the human body because of its similar structural and chemical properties with human tissues. It is the most stable calcium phosphate and show excellent biological properties. HA crystallises in hexagonal structure with lattice parameter value $a = 9.5\text{\AA}$ and $c = 6.8\text{\AA}$. The crystal structure of HA (**figure.3**) explains the hexagonal structure of PO_4^{3-} tetrahedron creating two kinds of tunnels parallel to the c - axis. The first type of tunnel like structure is filled with $\text{Ca}^{2+}(\text{A})$ ions which form CaO_9^- polyhedra, whereas the other type, which is lined by oxygen and other Ca ions, is occupied by OH^- anions. The second type of calcium ions forms the triangle at $z = \frac{1}{4}$ and $z = \frac{3}{4}$. Three ions of Ca^{2+} in the corners of the triangle is

bonded with central OH⁻ anion in the tunnel which is placed below or above of the triangular plane. [7,8]

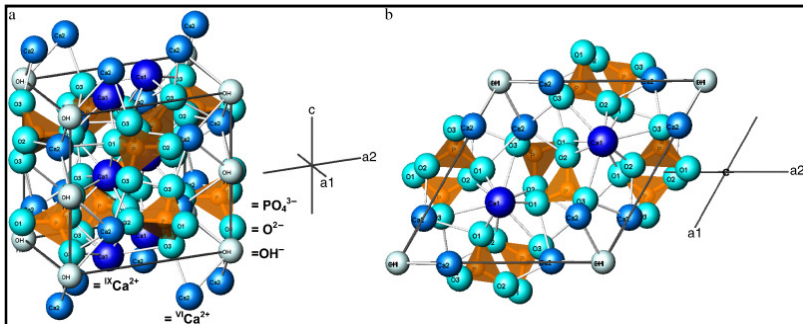


Figure 3: Crystal structure of hydroxyapatite after Wilson et al. projected perpendicular to c-axis. (b) Crystal structure of hydroxyapatite after Wilson et al. projected on (001). [7]

Within the CaP family HA shows an excellent biological capability and surface active nature with living tissues and organs and it has become one of the promising materials for biomedical application. Likewise, nano particles and porous based HA are good candidates for drug delivery and HA column is used for the separation of RNA and DNA from the biological samples. HA is also an efficient catalyst due to its astonishing properties

like ion exchange ability, adsorption capacity, non-toxicity, acidic base properties and thermal stability. [1,2,9–11]

The Ca/P ratio in HA is 1.67 and small variation in this value will affect the stability of HA in the temperature treatment. The lattice of HA can easily incorporate different types of substituent in the apatite structure, which in turn leads to the modification in crystalline properties, morphology, lattice parameter and thermal stability. It is proved that trace amount of cations (Mg^{2+} , Zn^{2+} , Sr^{2+} etc) and anions (SiO_4^{4-} , F^- , CO_3^{2-} etc) in apatite lattice plays a decisive role in its biological performance upon implantation. Different types of synthetic methods are used for the preparation HA, which depends upon the properties like, size, crystalline nature and shape of HA. Among them, precipitation, solid state, micro emulsion etc. are the main used strategies. [8, 12–14]

The fabrication of stable artificial bone implant interface is an important criterion for the success of dental and orthopaedic applications. The stability of implant material in the host body is influenced by some important parameters like design of the implant, recipient health, surgical technique and direct host implant effect. Different types of approaches have been developed to induce the favourable host to implant interactions, such as production of implant surface with microscopic irregularities, porous surface and osteoconductive coatings.[15–17]

Ti based alloys were widely used for orthopaedic implants because of its very high corrosion as well as fatigue resistance and its biocompatibility. Anyhow, less osteoconduction properties cause the encapsulation of Ti implants with fibrous tissue, which lag the healing process time. To overcome these limitations, Ti is employed with different surface modification processes to improve the osteoconductive properties. HA coating is widely used for the surface modification process and it helps to the faster bone regeneration compared to uncoated Ti surface. HA coating stimulates new bone ingrowths through osteoconduction mechanism without causing any local or systemic toxicity and induces the natural bone formation around the implant. [4, 18–22]

Nowadays, HA coatings are used for hip and knee replacing. Different coating process such as plasma spraying, sol-gel processing, electrical polarization, high-velocity oxy-fuel spray (HVOF) and aerosol deposition have been used to deposit HA coating onto Ti or its alloy substrate. Meanwhile, the long-term stability of HA coating is still a difficult problem. To overcome these problems, coatings should have good mechanical properties and high bonding strength interface between coating and metallic substrate. From the above coating techniques, plasma spraying has been successfully used as a reliable cost-effective solution and has attracted much attention in the recent years. [19]

It has been reported that, HA has a problem of very low biodegradation properties, which prevents the natural bone ingrowths for a longer time. The presence of β TCP increases the poor biodegradation properties of HA ceramics. The HA/ β TCP composite is expected to increase the bone growth without changing the osteoconductive properties of HA. [23,24]

1.6. Beta tricalcium phosphate (β TCP)

β TCP emerged as one of the most imperative biomaterials because of its astonishing properties in terms of biocompatibility, in-vivo bioactivity, bioresorbability and osteoconductivity [25–28]. According to Dickens' studies, the β TCP crystallises in the form of rhombohedral space group R3c with unit cell parameter $a = 10.44\text{\AA}$ and $c = 37.38\text{\AA}$ and the unit cell containing 21 formula units of $\text{Ca}_3(\text{PO}_4)_2$. The structure of β TCP can be disturbed by different layers of PO_4 tetrahedron and the Ca ion in the centres of this tetrahedron. **Figure 4** shows the crystalline structure of β TCP.

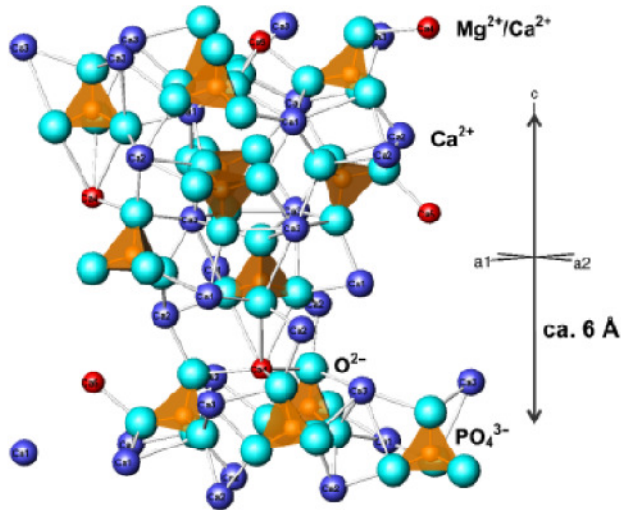


Figure 4: Crystal structure of β -tricalcium phosphate after Dickens et al. projected perpendicular to c-axis [7]

Recently, biphasic calcium phosphate came to use in bone graft application because of its higher resorbability compared to the pure HA components. One fundamental issue related to the processing and use of β TCP is the phase transformation (from β to α phase) at high temperature. As a matter of fact, tricalcium phosphate exists in three different allotropic phases, β ($T < 1180^\circ\text{C}$), α ($1180 < T < 1430^\circ\text{C}$) and α' ($T > 1430^\circ\text{C}$). Due to β to α phase transformation, bio-restorability of TCP is reduced and this is not desirable for its application. The phase transition also decreases the densification and, thereby, the mechanical strength. β to α phase transformation can be affected by the stoichiometric Ca/P ratio. Any small change in the Ca/P

ratio affects the purity of TCP in the form of β phase. Therefore, in order to utilize the properties of TCP for practical applications, it is necessary to stabilize the β -phase at a high temperature. [29–33]

The addition of mono- and divalent metal ions as dopants for TCP is found to stabilize the β phase at high temperature. The cations like (Mg^{2+} , Zn^{2+} , Sr^{2+} etc) and anions (SiO_4^{4-} , F^- , CO_3^{2-} etc) are used for the phase stabilization of β TCP. Human hard tissue (enamel, dentins and bone) in turn contains trace amount of elements like K, Na, Mg, F, K, Zn and CO_3 ions and hence this addition of metal ions will not affect the biological performance. **Table 4** shows the percentage of elements present in the human body. [26,32,34–36]

	Enamel	Dentine	Bone
Ca (wt.%) ^a	37.6	40.3	36.6
P (wt.%) ^a	18.3	18.6	17.1
CO ₂ (wt.%) ^a	3.0	4.8	4.8
Na (wt.%) ^a	0.70	0.1	1.0
K (wt.%) ^a	0.05	0.07	0.07
Mg (wt.%) ^a	0.2	1.1	0.6
Sr (wt.%) ^a	0.03	0.04	0.05
Cl (wt.%) ^a	0.4	0.27	0.1
F (wt.%) ^a	0.01	0.07	0.1
Zn (ppm) ^b	263	173	39 ^c
Ba (ppm) ^b	125	129	
Fe (ppm) ^b	118	93	
Al (ppm) ^b	86	69	
Ag (ppm) ^b	0.6	2	
Cr (ppm) ^b	1	2	0.33 ^d
Co (ppm) ^b	0.1	1	<0.025 ^d
Sb (ppm) ^b	1	0.7	
Mn (ppm) ^b	0.6	0.6	0.17 ^d
Au (ppm) ^b	0.1	0.07	
Br (ppm) ^b	34	114	
Si (ppm)			500 ^e
Ca/P ^f	1.59	1.67	1.65

Table 4: Percentage of elements presented in the human body. [80]

1.7. Doping of β TCP

Mg is one of the most common doping elements used for the biomedical applications because of its important role in biological systems. Mg associated biological apatite shows better performance than pure form. Reported studies showed that small amount of Mg (2mol%) enhances the bioactivity and biocompatibility of HA ceramics; Mg is also found in the human hard tissues. [28,33,37]

MgO is a commonly used dopant for the β phase stabilization of TCP. The presence of Mg in TCP also improves properties like biocompatibility, density, mechanical strength *etc* [26–28,32,38–41]. Pan et al. found that small amount of MgO in the β TCP structure enhances the phase stability and improves the biocompatibility of TCP [29]. Mg^{2+} ions replace calcium (Ca^{2+}) ions in β TCP structure and the obtained mineral phase is commonly known as whitlockite (β -TCMP) [38].

The phase diagram of MgO doped β TCP shows the effect of incorporation of Mg ions on the β TCP lattice. At the synthesis temperature of 1025°C up to ~14 mol% Ca ions can be replaced by Mg ions and due to this change the lattice parameter and crystallite size of β TCP is reduced.

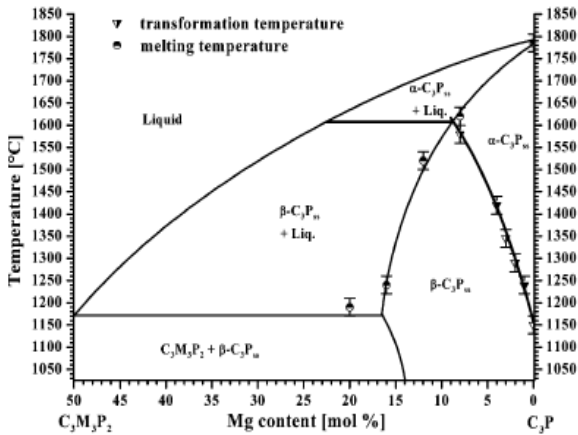


Figure 5: Phase diagram of MgO doped β TCP synthesized at 1120 $^{\circ}\text{C}$ [32]

The phase transformation temperature of β to α polymorph increased from 1150 $^{\circ}\text{C}$ without Mg^{2+} to 1540 $^{\circ}\text{C}$ with 8 mol% substitution on the Ca^{2+} site. Samples with larger substitution than 10 mol% sintered at the temperature below 1600 $^{\circ}\text{C}$ which implies that the further increase will not affect the phase transformation. [32] [42]

We have already seen the applications of CaP based materials particularly in orthopaedic and dental implantations. CaP based coatings are used now mainly for the artificial implantation of human joints. Plasma spray coating is one of the common techniques, which is used for the coating process. [43–45]

1.8. Plasma Spray Coatings

Thermal spraying techniques are well exploited coating process in multifunctional applications for industries. The main advantages of this type of coating are that advanced coating materials can be used and also coating and substrate material can be varied. Many surface problems of the materials can be resolved by this technique.

Plasma spray is one of the most versatile thermal spray coating processes. This process is capable of spray all types of sprayable materials. In plasma spray, powder materials or sometimes liquid, is fed into the gas plasma stream. The plasma is produced by striking an electric arc between a figure type tungsten (W) cathode and a nozzle type copper anode inside the plasma torch. [18,44–47]

The injected powder materials get melted because of the high temperature of plasma and highly accelerated samples were coated on the substrate surface for the development of lamellar structured coating. The high working temperature of the spray gases which is formed by the plasma process and the automation of plasma spray devices make it possible to produce high-quality coatings for a wide variety of applications. [15,43,48,49]

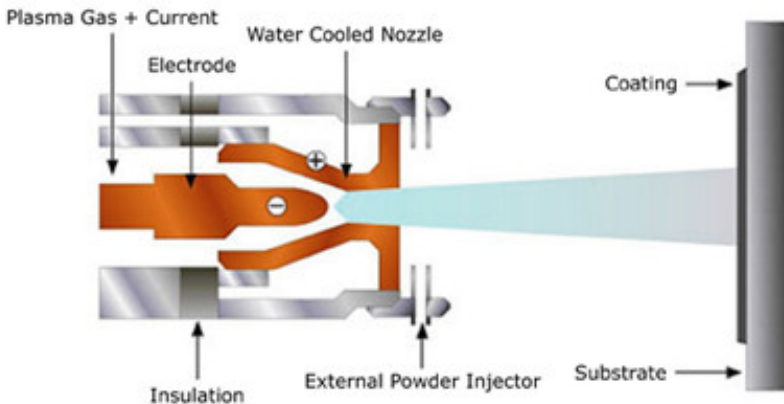


Figure 6: Process of plasma spray coatings

(Source: <http://www.advanced-coating.com/english/spraying-plasma.htm>)

Nowadays, plasma sprayed coatings are widely used for biomedical applications especially in the dental and orthopaedic implantation field. Previously, Ti based alloys were widely used for the orthopaedic and dental implant applications because of its high corrosion and good biocompatibility. Due to the limited osteoconductivity edges of Ti implants with fibrous tissues delays the healing time. To overcome these limitation's different types of surface modification processes are employed on the surface of Ti. The coating of HA is a widely used surface modification technique due to its excellent biological properties. HA is a well employed

bone graft material due to its similarity with human hard tissues. It is conceivable that plasma spraying of HA on the Ti surface is the most widely used technique due to its process simplicity, low-cost and bulk production. [6,20,43,46,49–56]

The present research focus on the modification of calcium phosphate coatings with improved bio-degradation properties. Beta tricalcium phosphate (β TCP) has been used in clinical applications for its good micro-porosity and higher biodegradation properties with respect to HA. Researchers have reported that the presence of β TCP helps to improve the properties of HA, like biocompatibility, osteoconductivity and biodegradation. In particular, the mixture of 40% of β TCP and 60% of HA produce better result than other compositions. [57–62] Based on these inferences, we decided to focus on the production of HA/ β TCP plasma sprayed coatings. The studies showed that the transformation of β to α phase during the plasma spray process takes place because of the very high-temperature formation. [15]

The aim of the present PhD work is to synthesize high temperature phase stabilized β TCP and HA/ β TCP powders for plasma spray coating applications and fabricate HA/ β TCP based coatings for the development of implantation processes.

Chapter 2: Materials and Methods

In the past, calcium phosphate powders were mainly prepared by three methods: solid-state synthesis, wet chemical method and hydrothermal route. Among these methods the solid-state synthesis allows an excellent composition control. Therefore, it is the most common method for the preparation of calcium phosphates [63]. Other synthesis methods require obeying several strict processing conditions like reaction temperature, time and solution pH; a slight variation of any of these conditions can cause the formation of other phosphate phases, which are undesirable.[29, 33, 35, 51] The synthesized powders find application in plasma spray coating for orthopaedic implants. The methods and procedures which used for the production of β TCP and HA/ β TCP plasma sprayed samples are explained below.

2.1. Solid state synthesis method

2.1.1. MgO-doped β TCP powder

MgO-doped TCP powder was synthesized by conventional solid-state reaction method. High-purity $\text{CaHPO}_4 \cdot 2\text{H}_2\text{O}$ (brushite- Sigma-Aldrich, 98%) and CaCO_3 (calcium carbonate-Sigma-Aldrich, 99%) with average grain size

of 5 μ m, were used in a molar ratio 2:1. The two raw powders and different amounts (0-14 mol%) of MgO (magnesium oxide- Farve s.r.l. Laboratories Pharmaceutics, 98.8% m) were mixed using a mortar and pestle, and further ethanol is added to obtain a homogeneous mixture. The obtained slurry was dried at 100⁰C for 12h before being transferred into an alumina crucible (capacity =50ml), subjected to heat treatment at 1000 – 1300⁰C for 2-12h and then freely cooled down to room temperature within the furnace.

2.1.2. HA/ β TCP (60:40) composite powders

The HA/ β TCP powders were synthesized using solid state method. Hydroxyapatite (HA) powder (Eurocoating, Italy) and 2 mol% MgO doped β TCP powders were used in 60:40 weight ratios. The as-received HA powder was heat treated at 1300⁰C/2h and mixed with β TCP using ethanol for homogenisation. The obtained slurry was dried at 100⁰C for 12h before being transferred into an alumina crucible (capacity =50ml), subjected to heat treatment at 1300⁰C for 2 hand then freely cooled down to room temperature within the furnace.

From the above synthesized powders, three powders were selected for the plasma spray process (Thanks to the collaboration with Eurocoating spa). The 1 mol% MgO doped β TCP powder is named as 'A', 2% MgO doped β TCP powder as 'B' and HA/ β TCP (60:40) is named 'C'.

Crystalline phase analysis was carried out by X-ray diffraction (XRD) (Rigaku DMax - Bragg-Brentano configuration). The measurement conditions were: range, $2\theta = 20-50^\circ$; step = 0.05° ; fixed time = 6 s; radiation = $\text{CuK}\alpha$.

The crystallite size of the powders was calculated by the Scherrer equation [64–66]

$$\text{crystallite size} = 0.9 \lambda / b \cos\theta \quad (1)$$

where λ = X-ray wavelength, θ = Bragg diffraction angle and b = X-ray peak broadening. The value of b was measured from the highest intensity peak width at half height.

The quantitative analysis of the samples was carried out by a computer software MDI-JADE and MAUD[21].

Fourier transformation - IR spectroscopy (FTIR) - Avatar 330 –Thermo Optics - spectra was recorded in transmission mode on KBr pellets, collecting 64 scans in the $4000-400 \text{ cm}^{-1}$ range, with 4 cm^{-1} resolution.

Thermo-differential analysis (DTA) - Netzsch, STA409- was carried out up to 1500°C using alumina crucibles with α -alumina powder as reference. The analysis was performed in static air with heating and cooling rates of $10^\circ\text{C}/\text{min}$. To explain some peaks obtained in the DTA curves, θ TCP pellets were also prepared for successive observations with Scanning Electron Microscope (SEM) (Jeol, JSM 5500). The synthesized powder was uni-

axially pressed using 13mm diameter die at 10 MPa pressure and subjected to heat treatment at 1500°C with a heating rate 10°C/min. Then the pellets were placed on a conductive adhesive tape over the aluminium sample holder. After being coated with a thin layer of Au-Pd layer by sputtering, the samples were inserted in the SEM chamber and observed at various magnifications by using 20 kV acceleration voltages.

Chemical analysis of the raw powders was carried out by inductively coupled plasma - atomic emission spectroscopy (ICP-AES) after the dissolution of a small amount of powder dissolved in hot 5wt% HNO₃ water solution and analysed using the instrument. Ultra pure (99.99%) hydroxyapatite (HA) powder was used as standard for Ca and P; a multi element standard (sol.IV, Merck) was used for the detection of the other elements.

After the heat treatment the powder was grinded using agate mortar.

For the granulation process, the powder was kept on a rotating surface and water-binder (B-1000, 5%) mixture was sprayed over it. The β TCP granules were collected and dried at 100°C. The dried granules were sieved using 100-150 μ m sieve. Then the powder was heat treated at 1100 °C for 2h with 2°C/min for the removal of binder. The heat treated powder was sieved and characterized by SEM, XRD and FT-IR.

For measuring the flowability of the granulated powders, a certain amount of powder was used for measuring the flow rate by the use of the Hall flow-meter funnel, by adapting the procedure described in ASTM B213 norm. As the powder does not flow unaided through the Hall flow-meter funnel; the funnel was connected to the columns of a sieve shaker - Endecotts Ltd, EVS-1 - operating at 60 and 80 Hz at a height of 16 cm from the base, thus aiding the flow of the powders through the orifice (2.54 mm diameter) of the funnel. The powder was poured in the funnel and the time required to exit completely from it was recorded. The Hall flow rate was evaluated using the equation given below:

$$FR_H^* = t / 25g \quad (1)$$

t being the flow time for 25 g of powder (instead of 50 g as in ASTM B213 norm due to the limited density of the powders considered here). **Figure 7** shows the images of flowability measurement.

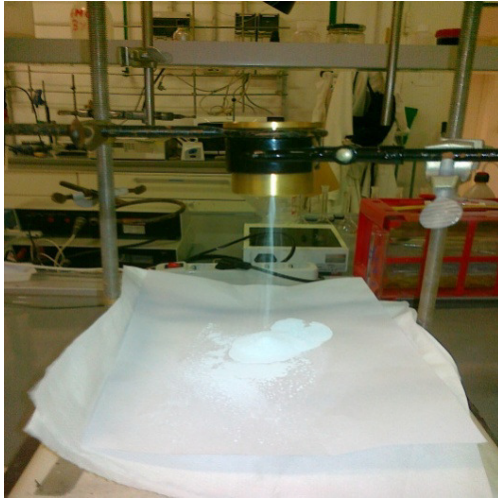


Figure 7: Flowability measurement

The apparent density of the powders was measured by using a procedure similar to that described in ASTM B703 - UNI EN 23923-2 norms by using a 35 ml cylinder.

From the synthesized powders, three types of calcium phosphate powders were selected for the plasma spray process. That are 1 mol% MgO doped β TCP, 2 mol% MgO doped β TCP and HA/ β TCP composite powder.

The granulated powders were used for plasma spray coating process. During the process, the β phase of TCP is transformed into α phase. For analysing the stability of α phase obtained in the coatings, the coated

samples were subjected to thermal treatment at different temperatures and holding time. The plasma sprayed samples were heat treated at 500-1100°C for 15 min to 2h and then freely cooled down to room temperature within the furnace. After the thermal treatment the samples were characterized using SEM, XRD, FT-IR, ICP analysis etc.

2.2. Invitro analysis

2.2.1. Bioactivity behaviour

In vitro bioactivity properties were analysed by soaking the plasma spray coated samples in SBF at 37°C for 1 – 4 weeks. The calcium phosphate coatings obtained after thermal treatment was used for the bioactivity measurements. The average coating thickness of the sample is 80 - 90 µm. 2 cm slices were cut from the plasma sprayed samples and were immersed in 50 ml SBF for 1- 4 weeks. For the preparation of SBF solution same method used in Oyane et al. [67]

All the apparatus used for the preparation of the SBFs was washed with 1.0M HCl and ultra pure water. 700 ml of double distilled water was poured in to a 2000 ml beaker, and stirred using a magnetic stirrer at 37°C. The temperature was measured using a laboratory thermometer. Once the liquid temperature reaches 37°C, the reagents were dissolved in water in

the sequence listed in the **Table 5**. The HEPES buffer was previously dissolved in 100 ml distilled water before adding to the solution. [4]

Reagent	Purity / %	Amount
NaCl	>99.5	5.403 g
NaHCO ₃	>99.5	0.740 g
Na ₂ CO ₃	>99.5	2.046 g
KCl	>99.5	0.225 g
K ₂ HPO ₄ ·3H ₂ O	>99	0.230 g
MgCl ₂ ·6H ₂ O	>98	0.311 g
HEPES	>99.9	11.929 g
CaCl ₂	>95	0.293 g
Na ₂ SO ₄	>99	0.072 g
0.1M NaOH	-	0.8 ml

Table 5: Reagent, purity and amounts for preparing 1000 ml of SBF solution

2.2.2. Solubility Measurements

pH 5.5MES buffer solution: 1.0 mol MES [2-Nmorpholino) ethane sulfonic acid] having a pH of 5.5 at 37°C and containing 8×10^{-5} mol NaCl, 8×10^{-5} mol CaCl_2 , and 5×10^{-5} mol K_3PO_4 and sodium azide (0.1 wt %) as bacteriostat. pH is adjusted to 5.5 by addition of 0.1 mol NaOH solution.

100 mg of coating is added to 100 cm³ of each buffer solution (solid/liquid ratio of 1 mg/ml). This suspension is equilibrated in capped 250 cm³ polyethylene bottles and kept at 37.0 ± 0.1 °C with a continuous shaking. Estimated equilibration time is 4 weeks (28 days). The pH of each suspension is obtained each day. The pH measurement is carried out in the suspensions in original bottles shaken in a bath at 37°C. The measurements in standard buffer solutions are done in the same manner, and they are carried out before, in between and after sample measurements. Each day a volume about 0.5 ml to 1 ml (volume depends on the concentration of Ca and P determined on the previous day) of suspension will be taken from the bottle using ICP.

Chapter 3: Results and Discussions

3.1. Solid state Synthesis

3.1.1. MgO doped β TCP powder

MgO-doped TCP powder was synthesized by the solid-state reaction method. The aim of the present work is to produce high temperature phase stabilized β TCP powders and evaluate the maximum chemical substitution of Mg^{2+} in β TCP structure as a function of synthesis temperature.

Mineralogical analysis of the synthesized powders

The XRD patterns of MgO-doped TCP powder synthesized at different temperatures (1000-1300 °C/2h) are shown in **Figure 8**. The narrow peaks observed in the spectra represent the crystalline nature of the powders and correspond to β TCP phase with rhombohedral crystal structure (whitlockite - 009-0169) [28,39,68]. For 1000 and 1100°C synthesis temperature, no extra peaks are observed and this suggests that only β TCP phase is obtained for any MgO additions (1-14 mol %) at such synthesis temperatures. This observation is in agreement with previous studies [32,41]. Conversely, for synthesis temperature of 1200 and 1300°C an

additional peak is detected at $2\theta=31.7^\circ$ starting from 5 mol% MgO doping; such peak corresponds to hydroxyapatite (HA- $\text{Ca}_5(\text{PO}_4)_3(\text{OH})$ - 09-0432) phase. The quantitative analysis of the crystalline phases allows to estimate a consistent increase in HA phase concentration with MgO doping at 1200 and 1300°C/2h synthesized samples.

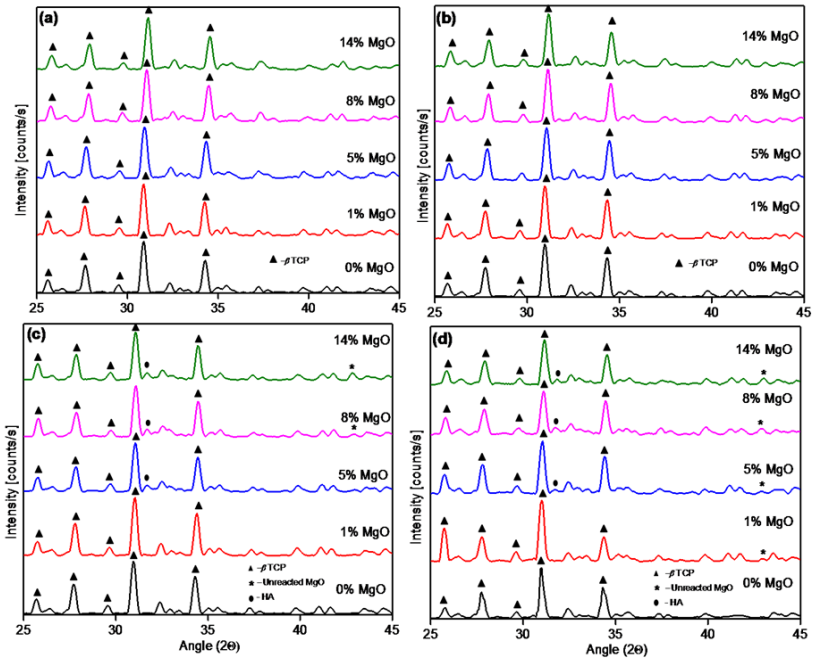


Figure 8: Crystal structure of hydroxyapatite after Wilson et al. projected perpendicular to c-axis. (b) Crystal structure of hydroxyapatite after Wilson et al. projected on (001). [7]

Figure 9 reports the HA amount as a function of MgO concentration in TCP powders synthesized at 1300°C for 2h as calculated by MAUD software. It shows that β TCP is the only crystalline phase up to 2 mol% doping and a significant concentration of 8 wt% HA phase is observed in 5 mol% MgO-doped TCP powders. For 14 mol% MgO-doped powders, the percentage of HA are 15%. Also the TCP powder synthesized at 1200°C for 2h shows similar behaviour and these points out that an increase in dopant concentration increases the formation of HA phase.

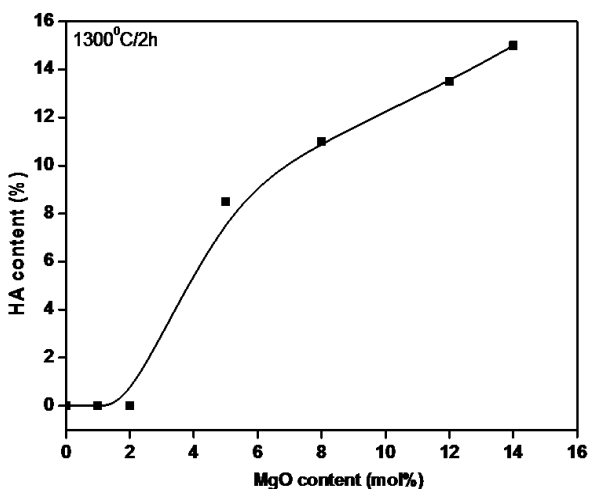


Figure 9: Hydroxyapatite (HA) content as a function of MgO addition in powder synthesized at 1300°C for 2h.

As shown in **Figure 8 (c)**, at the highest doping levels (8 and 14 mol %) for synthesis temperature of 1200°C, an additional peak at $2\theta = 43^\circ$ is observed, which corresponds to MgO (Periclase-45-0946). For the

Synthesis temperature of 1300°C, the MgO peak begins to appear at a lower MgO concentration (1 – 5 mol %). Presumably, the separate MgO peak corresponds to reaching the solubility limit and thereby to the segregation as third phase at such synthesis temperatures. Conversely, at lower processing temperature (1000 and 1100°C), there is no un-reacted MgO for doping loads up to 14 mol%.

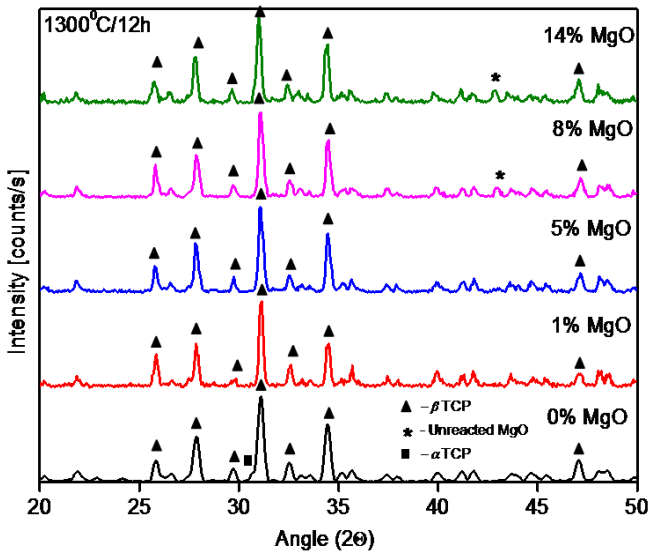


Figure 10: XRD analysis of β TCP powders synthesized at 1300°C/12h.

The presence of HA in the powders obtained after 2 h treatment shall be considered as a reaction intermediate only. In fact, no HA peaks can be detected in XRD spectra recorded on powders synthesized at 1300°C for 12 h (**Figure 10**). FT-IR analysis confirms the formation of HA phases in the 2h synthesized samples and its dehydroxylation after 12h treatment.

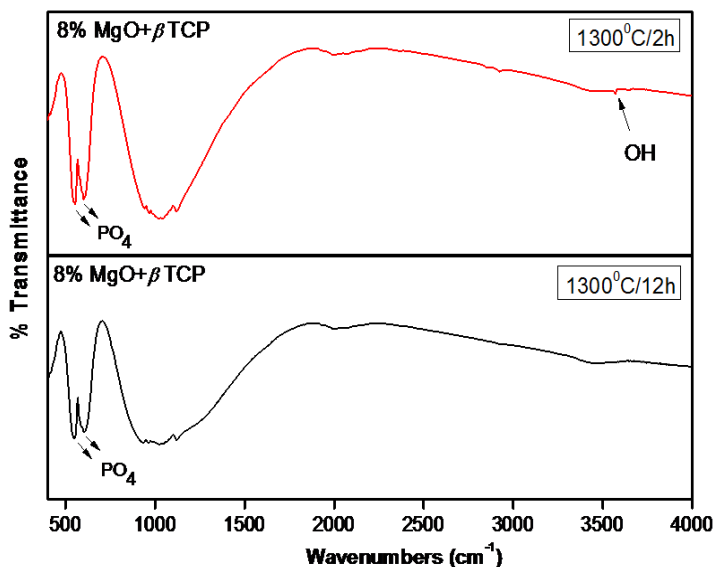


Figure 11: FT-IR spectra of 8 mol% MgO-doped β TCP synthesized at 1300°C for 2h and 12h.

Figure 11 shows the FT-IR patterns of 8 mol% MgO-doped β TCP powder synthesized at 1300°C for 2h and 12h: weak OH vibration peaks can be detected at 3575 cm^{-1} only for the 2 h treatment sample. On the other hand, the FTIR spectra of 12h synthesised sample shows the disappearance of OH vibrational peak at 3575 cm^{-1} and confirms the instability of HA phase.

The results obtained in the present work point out a certain disagreement with results previously reported, especially in Ref. [32]. The use of different raw materials and experimental conditions can account for such discrepancies. Nevertheless, additional analysis and studies are certainly required to clarify them.

A magnified portion of the XRD spectrum for pure and 8 mol% MgO-doped samples synthesized at 1300°C is shown as an example in **Figure 12**. It shows a clear shift of the peaks towards higher 2θ values for MgO doped β TCP samples. This peak shift is indicative of variations in the lattice parameter, which occurs because of the incorporation of Mg^{2+} ions into the Ca^{2+} sites of the host lattice. Also the width of the peaks is different, also demonstrating a change in the crystalline size.

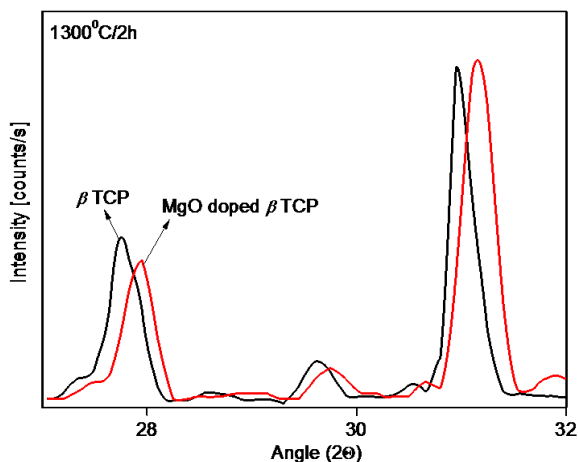


Figure 12: Peak shift due to the incorporation of 8 mol% Mg^{2+} into the βTCP lattice.

The variations in the lattice parameters and crystallite size affected by the addition of Mg^{2+} are reported in **Table 6** and **Figure 13**. For synthesis temperature of 1300°C, there is a consistent decrease in the lattice parameters ' a ' and ' c ' with MgO doping; up to 8 mol% and higher concentration the values remain constant. This decrease is associated with the substitution of Ca^{2+} ion (ionic radius: 0.9Å) by smaller Mg^{2+} (0.69Å). The crystallite size of the doped sample is shown to follow the same, if not more evident trend. At lower synthesis temperature the lattice parameters ' a ' and ' c ' show also a consistent decrease with MgO content. At 1200°C the lattice parameters ' a ' and ' c ' decrease from 10.44 Å to 10.39Å and 37.45Å to 37.3Å, respectively.

<i>Mg (mol%)</i>	<i>Lattice parameters</i>		<i>Crystallites size (nm)</i>
	<i>a (Å)</i>	<i>c (Å)</i>	
0	10.43	37.39	32.2
1	10.42	37.38	30.1
5	10.41	37.35	24.8
8	10.39	37.30	24.1
10	10.38	37.29	24.1
12	10.38	37.29	24.2
14	10.38	37.29	24.0

Table 6: Effect of MgO content on the lattice parameters and crystallites size of β TCP synthesized at 1300°C.

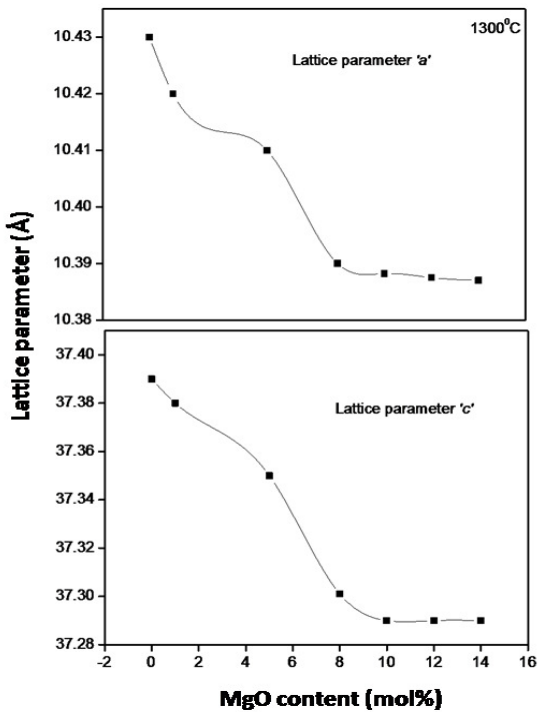


Figure 13: Effect of MgO incorporation on the lattice parameters of β TCP synthesized at 1300°C.

Thermal behaviour

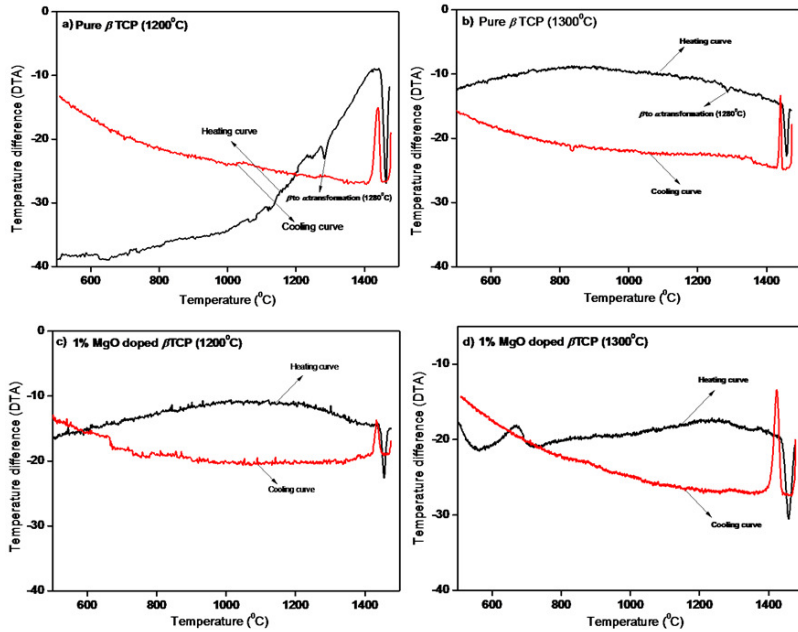


Figure 14: DTA of β TCP powder synthesized at 1200 and 1300°C.

Figure 14 shows the DTA plot of pure and 1 mol% MgO-doped β TCP powder synthesized at 1200 and 1300°C. The plot represents the behaviour on heating and cooling. For pure β TCP an endothermic peak is observed at 1280°C upon heating where as no exothermic peak is shown in the same temperature range upon cooling in both the cases; such peak can be associated to the β to α phase transformation of pure TCP. Also in

previous studies, such phase transformation is reported by an endothermic peak although observed at lower temperature (1180°C). In addition, no peak has been reported upon cooling around ~1180°C this pointing out the low temperature stability or meta-stability of the α phase [32]. The difference in the transformation temperature observed here with respect to previous results can be associated with the presence of Mg^{2+} in the powder precursors as impurity. As a matter of fact, ICP analysis of powder precursors (brushite and CaCO_3) revealed the presence of 0.32 mol% Mg^{2+} ions as impurity (no other impurities were found in concentration larger than 50 ppm). Similar observations on the transformation temperature associated with the presence of Mg impurities are also reported in other papers[29]. For 1 mol% MgO-doped β TCP no endothermic peaks are observed up to 1400°C and this can be associated with the stabilization of β phase at high temperature due to MgO doping. Similar behaviour was also observed for β TCP powders containing higher amount of MgO and at lower processing temperature.

In **Figure 14** an endothermic peak centred at 1465°C and an exothermic one at 1439°C are also evident on heating and cooling curves, respectively. These could be associated either to α to α' phase transformation or to a melting-solidification process whose nature is any how obscure with the data available here. Also in the present case a certain disagreement is pointed out with respect to previous studies although the impurity of the raw materials can only partially account for it. To analyse the possible

melting-solidification process, the TCP pellets were used for SEM analysis. **Figure 15** shows SEM micrographs of pure β TCP pellets synthesized at 1300°C and then treated at 1500°C: a fully dense morphology with properly connected grains of average size around 5 μ m. Conversely, the grain boundaries are not clearly visible in the sample treated at 1500°C and the microstructure resembles that obtained after a liquid phase - sintering phenomenon, with rounded pores and grains. On this basis the peaks recorded at 1465°C (heating) and 1435°C (cooling) in the DTA plots could be associated to a partial melting-solidification process.

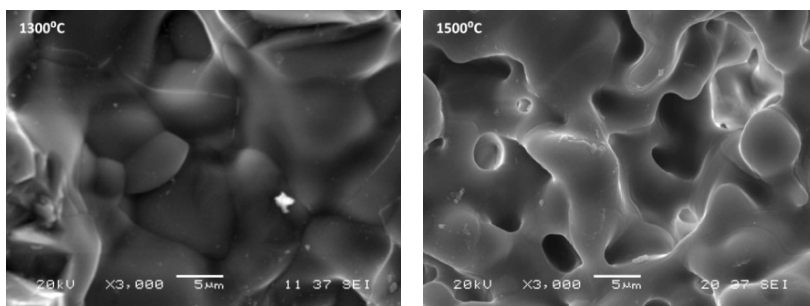


Figure 15: SEM images of synthesized and heat treated pure β TCP pellets

Samples with higher MgO concentrations could not be investigated by thermal analysis method since 1 mol% Mg²⁺ delays the transformation temperature above 1500°C, which is the limit of the instrument used in the current work.

The thermal stability of MgO-doped powders synthesized at 1300°C was analysed by high temperature treatments. Some samples were therefore heat treated at 1500°C for 4h and then analysed by XRD. The phase composition of the samples after heat treatment is shown in **Table 7**. Pure TCP powder contains 17.7% ' α ' phase, whereas samples doped with 1 mol% and above consist of β phase only at 1500°C. In samples with MgO concentration of 8 mol% and above, a mixture of δ TCP phases and MgO is observed, which confirms the reaching of the solubility limit of MgO in the β TCP which is lower than that previously proposed. [32]

<i>Mg (mol%)</i>	<i>Percentage composition (wt%)</i>		
	β TCP	α TCP	MgO
0	82.3	17.7	0
1	100	0	0
5	100	0	0
8	90.3	0	9.7
14	83.5	0	16.5

Table 7: Mineralogical composition of β TCP powder synthesized at 1300°C for 2 h and heat treated at 1500°C.

Based on the previous reports on the cytotoxicity of excess Mg content, we decided to further explore the work with lower concentration of Mg (1 and 2 mol%).

3.1.2. HA/ β TCP composite powders

The HA/ β TCP composite powder was produced by the mixing of HA powder and high temperature phase stabilized β TCP powder (2% MgO doped β TCP). The obtained powders were characterized using conventional techniques.

The XRD pattern of as received and heat treated HA raw material used for the production of HA/ β TCP composite a powder is shown in **figure 16**. The spectrum is matching with JCPDS. No. Hydroxyapatite - 09-432 – $\text{Ca}_5(\text{PO}_4)_3\text{OH}$ phase. The spectra clearly show the crystalline nature of the powder with respect to the effect of temperature. That is the heat treated powder has more crystalline nature compared to the as received HA powder. The crystalline size of the powder also increases with increase of temperature. The as-received and heat treated HA, crystal size calculated by Scherrer equation are 9.7 nm and 40 nm respectively, and this is due to the grain growth of HA crystals during high temperature treatment.

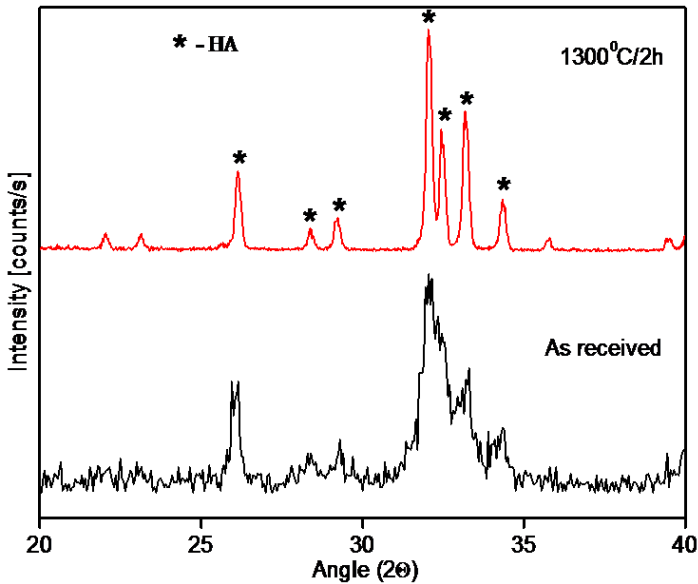


Figure 16: XRD spectrum of as received and heat treated HA powder

The treated HA powders are used for the preparation of HA/ β TCP composite powders. In the XRD spectrum (*figure 17*) of synthesized HA/ β TCP powders both the phases of HA and β TCP can be observed clearly. The peaks obtained at 2θ value 31.8° is matching with main intensity peaks (2 1 1) of HA (Hydroxyapatite - 09-432 – $\text{Ca}_5(\text{PO}_4)_3\text{OH}$) and peak value at 31.1° is (0 2 1) of β TCP (whitlockite- 09-0169- $\text{Ca}_3(\text{PO}_4)_2$).

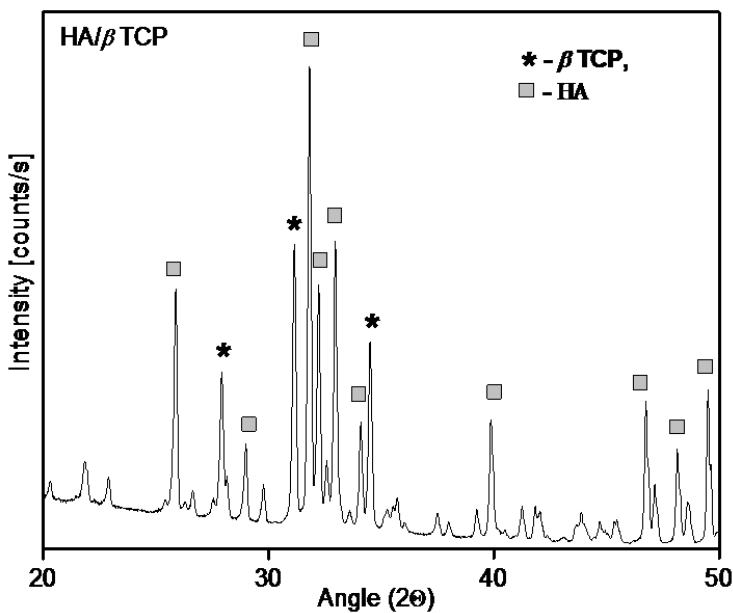


Figure 17: XRD spectrum of synthesized HA/ β TCP powder

The quantitative analysis of each phase obtained after MAUD analysis is explained in **figure 18** and **table 8**. From MAUD analysis it is evident that HA phase is 59% and β TCP is 41%.

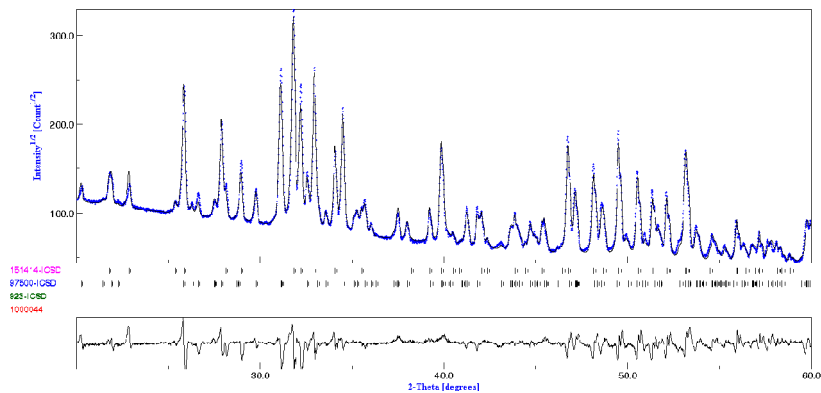


Figure 18: XRD plot obtained after MAUD analysis

<i>Powder</i>	<i>HA</i>	<i>βTCP</i>	<i>αTCP</i>
HA/ β TCP	59.1	40.9	0

Table 8: Percentage of considered phases obtained after MAUD analysis

3.1.3. Granulation of synthesised powders for plasma spray

The powders were produced with a view for the utilisation in plasma spray coating. The irregular shape of the synthesized powders (**figure 19**) is not satisfying the required properties for plasma spraying machine. For plasma spraying the powders should be within the granulometric size of 100-150 μ m.

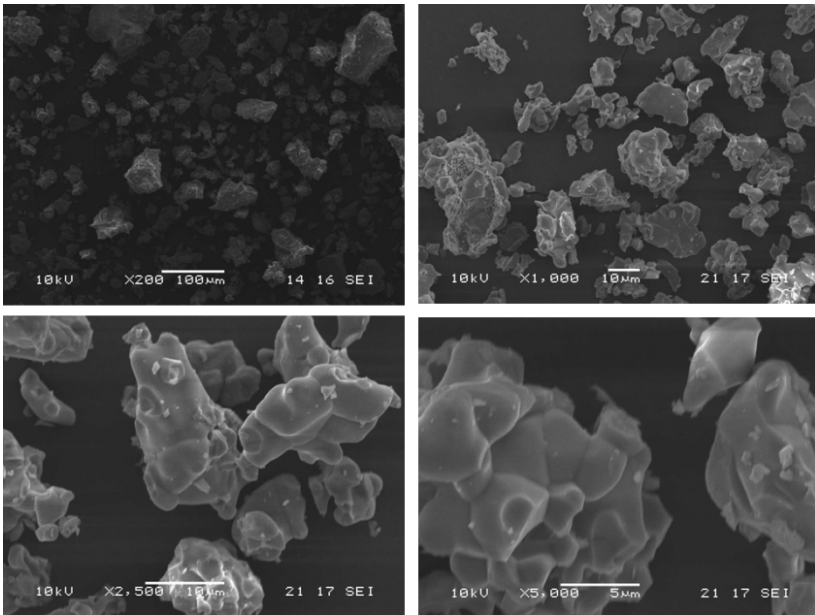


Figure 19: SEM images of the powders before granulation

For obtaining specific properties, the synthesized powders were subjected to granulation process. After the granulation process, the particles are agglomerated and a uniform shape was obtained in the size range 100 – 150 μ m. **Figure 20-22** shows the SEM images of the granulated powders. Three different types of powders were used for the granulation process and plasma spray coating. The 1 mol% MgO doped β TCP powder is named as 'A', 2% MgO doped β TCP powder as 'B' and HA/ β TCP (60:40) is named 'C'.

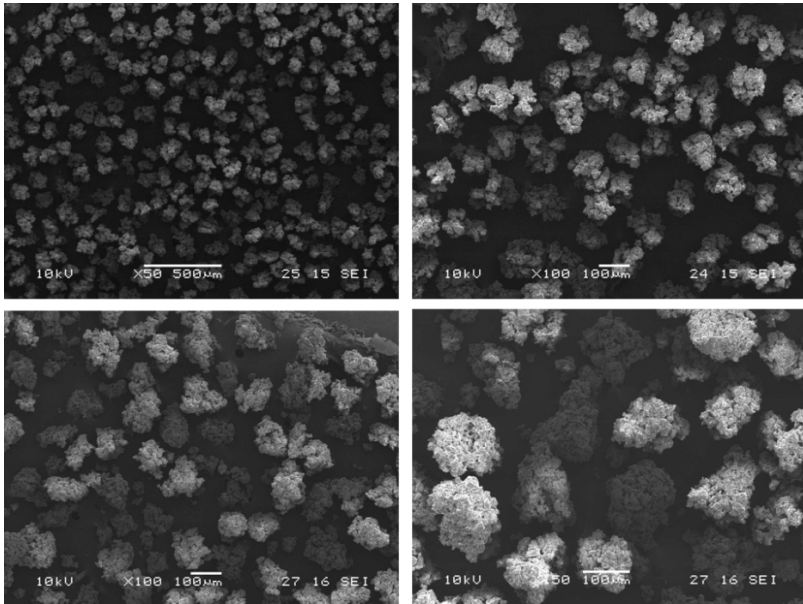


Figure 20: SEM images of the sample A after granulation process

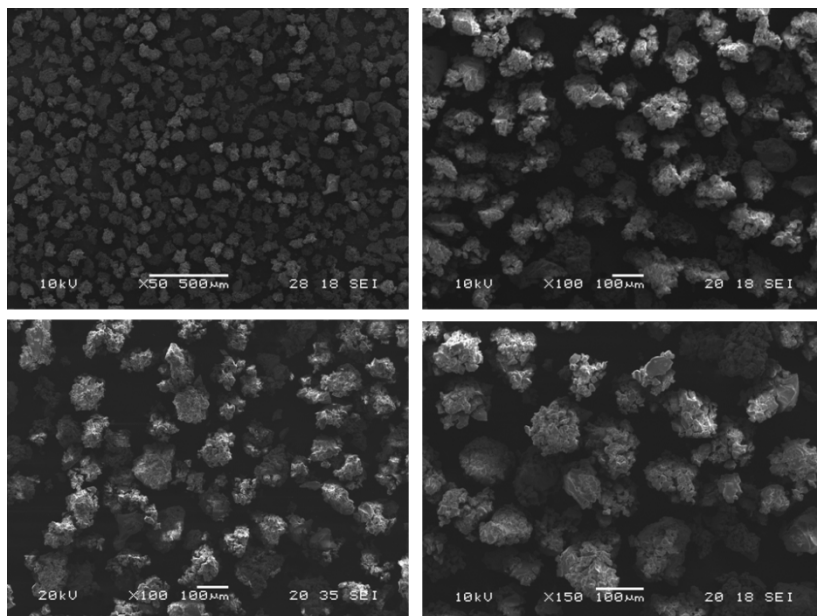


Figure 21: SEM images of the sample B after granulation process

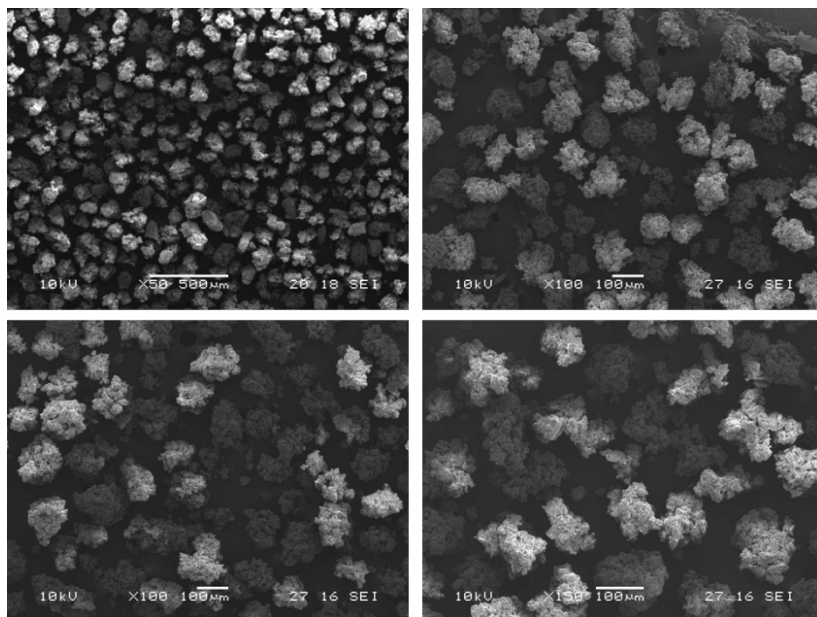


Figure 22: SEM images of the sample C after granulation process

3.1.4. Properties of granulated powders

The phase compositions of the granulated powders obtained by MAUD analysis is shown in **table 9**.

<i>Powder</i>	<i>HA</i>	<i>βTCP</i>	<i>αTCP</i>
A	0	100	0
B	4	96	0
C	59.1	40.9	0

Table 9: Phase composition in each sample after MAUD analysis

Powder 'A' shows 100% purity in β TCP phase; conversely powder 'B' contains 96% β TCP and 4% HA. The formation of HA in MgO doped β TCP powders has been previously explained.

The Infrared spectra of considered samples are shown in **figure 23**. The vibrations obtained 473, 570 and 605 cm^{-1} corresponds to PO_4^{3-} groups. The peak obtained at 3570 cm^{-1} in powder C represents the OH stretching

of HA. In samples 'A' and 'B' no such kind of vibrations was observed, even though powder 'B' shows small amount (4%) of HA phase in XRD.

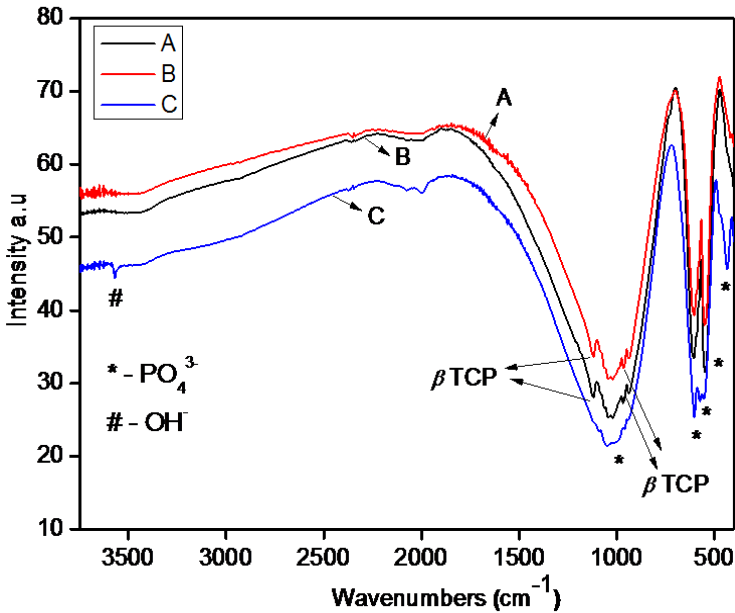


Figure 23: FT-IR spectrum of considered sample before plasma spray process

The strong bands in the IR spectrum can be attributed to PO_4^{3-} groups. The band at 1050cm^{-1} is due to the components of triply degenerated anti symmetric P-O stretching mode. The peak at 962 cm^{-1} is the non-

degenerated P-O symmetric stretching mode. The bands at 605cm^{-1} and 570 cm^{-1} are assigned to the components of triply degenerated O-P-O bending mode. Absence of any distinct band in the range of $1400\text{-}1550\text{ cm}^{-1}$ indicates that the samples do not contain large quantities of carbonate ions. The band due to the hydroxyapatite OH stretching vibrations at 3570cm^{-1} is visible on the FT-IR spectra corresponding to the HA containing sample C. IR spectrum contains some features according to β TCP phase observed from the band shoulders around 947 , 974 and 1120 cm^{-1} in sample 'A' and 'B'. A very weak peak is obtained at this range because of the presence of HA in sample C.[69, 70]

3.1.5. Flowabilty and density

The flowabilty and density are important factors for powders which are used in plasma spray process. The measured properties are reported in **table 10**

<i>Powder</i>	<i>Frequency (Hz)</i>	<i>Time (s) ± 5</i>	<i>FR_H ± 0.2</i>	<i>Bulk density(g/cm³)</i>	<i>Ca/P ratio</i>
A	80	74	2.96	1.1	1.47
	60	78	3.12		
B	80	113	4.52	0.8	1.49
	60	170	6.8		
C	80	109	4.36	0.8	1.58
	60	122	4.88		

Table 10: Flowabilty and bulk density of the powders

It is evident that powder 'A' shows better flowabilty rates compared to the other two powders because of the high bulk density. Higher MgO concentration reduces the bulk density. Ca/P ratio was obtained by ICP analysis. Sample 'A' and 'B' show Ca/P ratio as 1.47 and 1.49 respectively in good agreement with previous reports. In powder 'C' the obtained ratio is 1.58, because of the presence of both the phases of HA and β TCP.

The powders were used in the plasma spray machine (sample A, B and C) and coated on Ti surface. **Figure 24** show the images of the plasma sprayed coatings. **Sample D** is the pure HA plasma sprayed coating obtained from Eurocoating spa. The synthesized powders show good performance in the plasma spray machine and coatings are uniform.

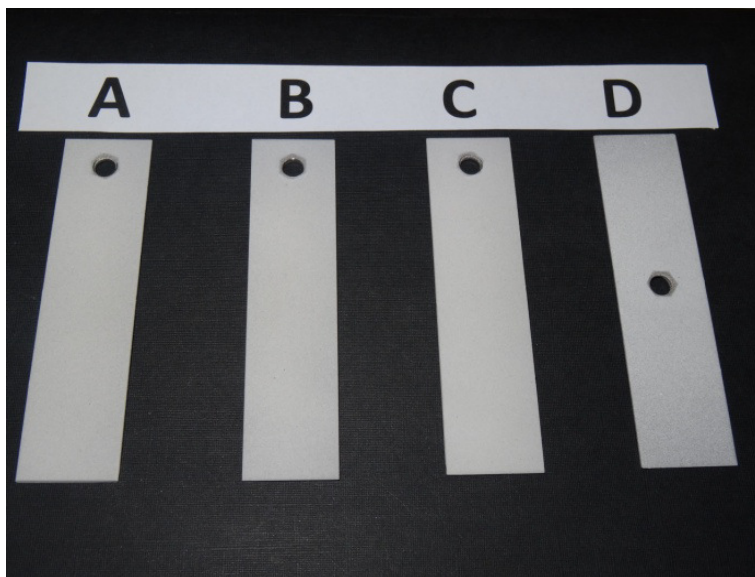


Figure 24: Images of plasma sprayed samples

3.1.6. Properties of CaP based plasma sprayed coatings

XRD spectra obtained after plasma spray process is shown in **figure 25** and the phase composition of each phase (calculated using MAUD) is given in **table 11**.

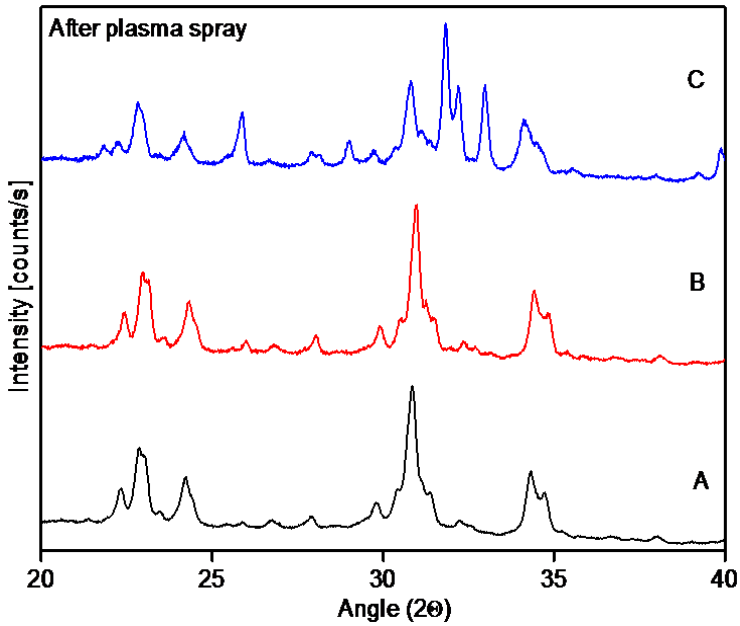


Figure 25: XRD spectra of considered samples after plasma spray process

The XRD spectra of sample 'A' and 'B' are matching with JCPDS. No. 09-348 – $\text{Ca}_3(\text{PO}_4)_2\text{OH}$ (α TCP) phase. The higher intensity peak observed at $2\theta = 30.7^\circ$ is the (1 7 0) phase of α TCP. This indicates that, after plasma spray process the β phase of TCP is transformed to α . The β TCP phase in sample 'C' also follows the same trend. The quantitative analysis of the samples obtained after MAUD analysis is shown in the **table 11**.

<i>Powder</i>	<i>HA</i>	<i>βTCP</i>	<i>αTCP</i>
A	0	33	67
B	1.5	20	78.5
C	47.3	7.5	45.2

Table 11: Percentage of phase compositions of the samples after plasma spray obtained after MAUD analysis

In the case of sample 'A', the β to α phase transformation is 67% and 78.5% in 'B'. But in 'C', after plasma spray 47.3% of HA, 45.2% of α phase and only 7.5 % of β is obtained. The initial powder had 60% of HA phase and 40% β TCP phase which implies that after plasma spray HA phase also shows some phase transformation to α TCP.

From the observations, during the plasma spray process, the higher temperature phase stabilized β TCP powders also changed their phase to α TCP due to the very high temperature formation and fast cooling rate.

FT-IR spectra of plasma sprayed samples are shown in **figure 26**.

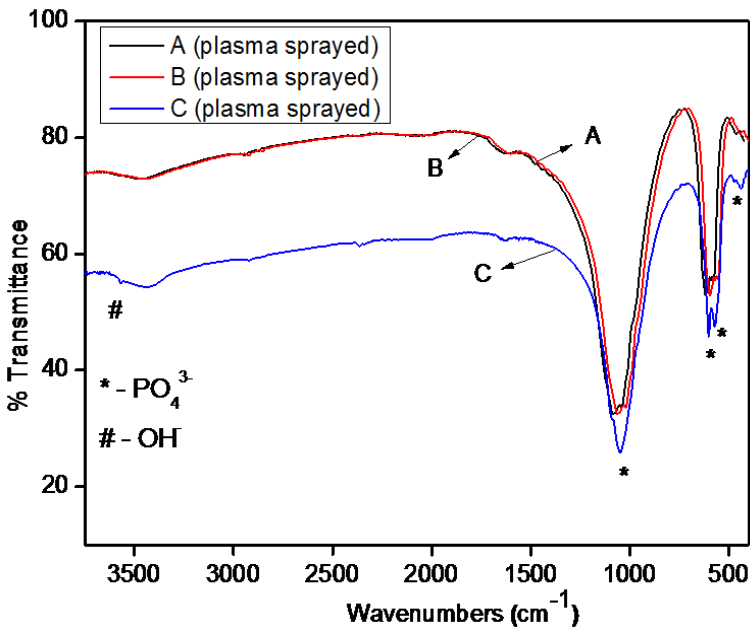


Figure 26: FTIR spectra of considered samples after plasma spray

After plasma spray the β TCP peaks of initial samples are completely disappear and the small vibrations observed at 603, 1032 and 1072 cm^{-1} indicates the formation of α TCP phase in all the samples. The OH vibrational peaks of HA is obtained at 3572 cm^{-1} in sample 'C'. The vibrations observed at 477, 566 and 609 cm^{-1} corresponds to PO_4^{3-} groups and a small shift of PO_4^{3-} vibrations can be seen after plasma spray. [69][70]

ICP analysis also shows small variations in Ca/P ratio from the initial results. The Ca/P ratio decreases from 1.47 to 1.45 in sample 'A', from 1.49 to 1.43 in 'B' and 1.58 to 1.51 in sample 'C'. This may be due to the phase transformation of TCP or melting of samples during plasma spray process.

SEM analysis of the coated sample cross section reported in **figures 27- 29**. They reveal that the coatings are uniform and well adherent with Ti substrate. The average coating thickness of the coatings is $\sim 80 - 90 \mu\text{m}$. For taking the cross sectional SEM images, the sample were moulded in an epoxy resin (Epofix resin and Epofix hardner in 5:1 ratio).

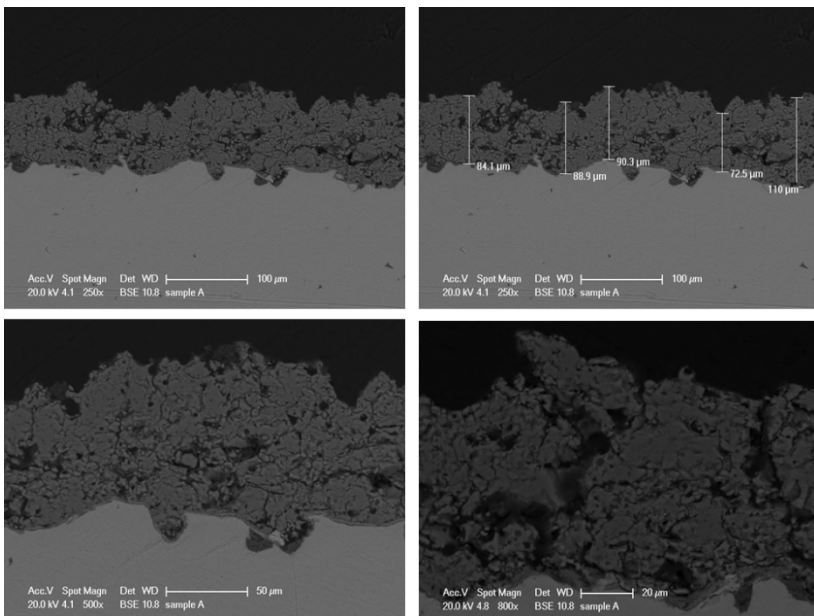


Figure 27: Cross section images of 'sample A' coated on Ti surface

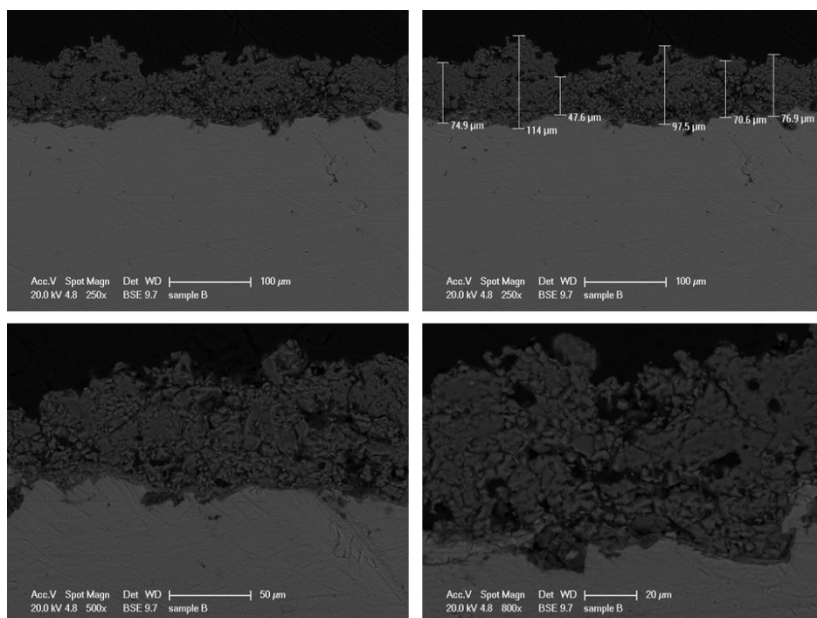


Figure 28: Cross section images of 'sample B' coated on Ti surface

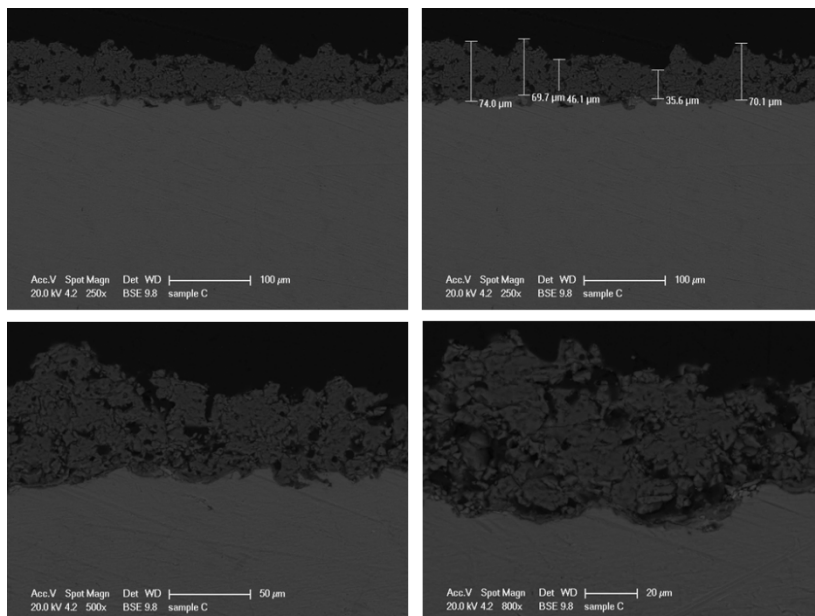


Figure 29: Cross section images of '*sample C*' coated on Ti surface

The melting of the samples can be clearly understood from the SEM images of the coated surface. **Figure 30 - 32** shows the surface SEM images of considered samples on the Ti surface.

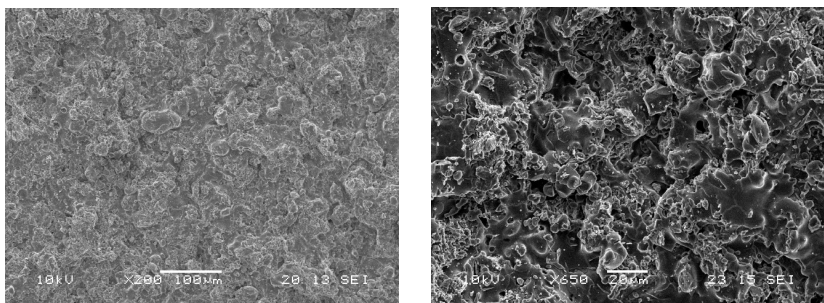


Figure 30: Surface SEM images of *Sample 'A'* coated on the Ti surface

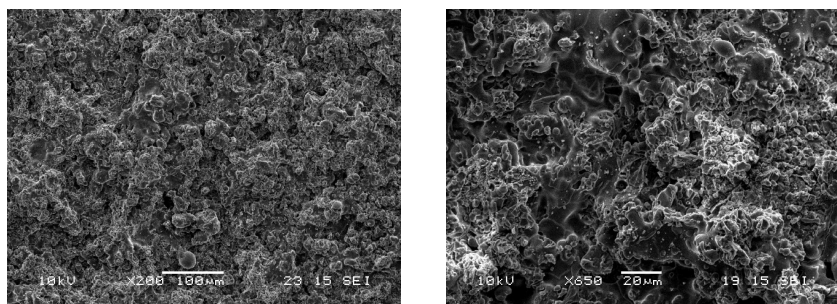


Figure 31: Surface SEM images of *Sample 'B'* coated on the Ti surface

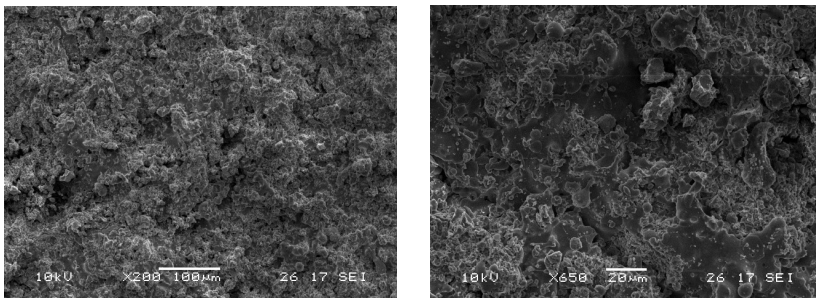


Figure 32: Surface SEM images of *Sample 'C'* coated on the Ti surface

As shown before, after plasma spray the β phase of TCP is transformed to α phase due to the very high temperature and fast cooling rate during the process. For analysing the stability of the obtained α phase after plasma spray coatings, the coatings were subjected to heat treatment in between the temperature range 500-1100°C for 15 min to 2h. After the thermal treatment the coatings were characterized using XRD, SEM, ICP and FT-IR. The properties of coatings obtained after thermal treatment is explained below.

3.1.7. Properties of coatings after thermal treatment

Initially, the **Sample 'B'** was used for the thermal treatment process. The XRD spectra of 2% MgO doped (B) coatings after thermal treatment is shown in **figure 33**. The spectra clearly indicate the reverse phase transformation of β TCP with respect to temperature.

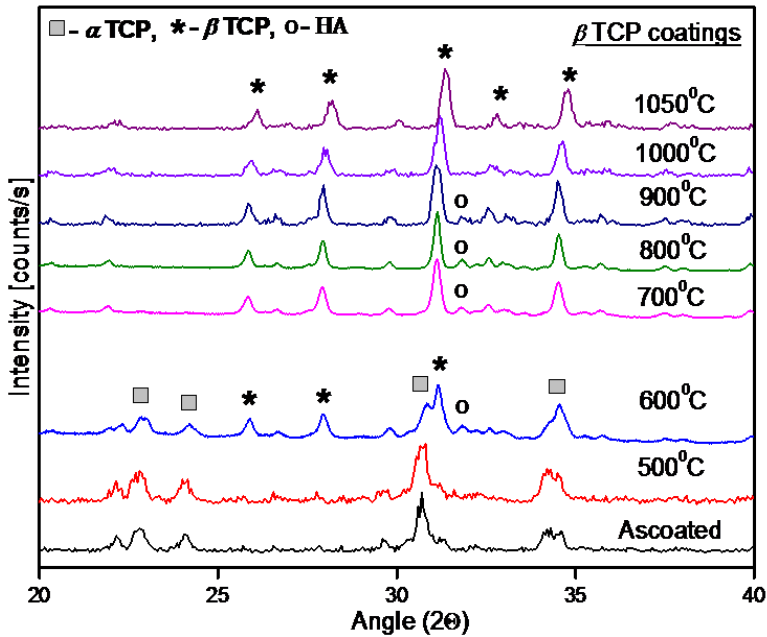


Figure 33: XRD spectra of coating heat treated at different temperatures

The percentage of each phase formation during thermal process obtained from MAUD analysis is given in **Table 12**. The table shows that the reversible phase transformation of ' α 'TCP with respect to the increase of temperature. At 800°C the ' α ' phase is completely removed and obtained β TCP and HA.

<i>Temperature (°C)</i>	<i>HA</i>	<i>βTCP</i>	<i>αTCP</i>
500	3.1	15.8	80.9
600	15.5	43.3	41.2
700	14.4	81.1	4.0
800	16.9	83.1	0
900	8.9	91.1	0
1000	3.0	97,0	0
1050	0	100	0

Table 12: phase composition after each specific thermal treatment

The phase transformation of α to β TCP is again confirmed with DTA analysis. **Figure 34** shows the DTA spectra of plasma sprayed TCP powder of **Sample B**.

Upon heating, an endothermic peak is observed at 550°C, which can be attributed to α to β phase transformation of plasma sprayed TCP. These DTA results are matching with the XRD results which we obtained during the heat treatment.

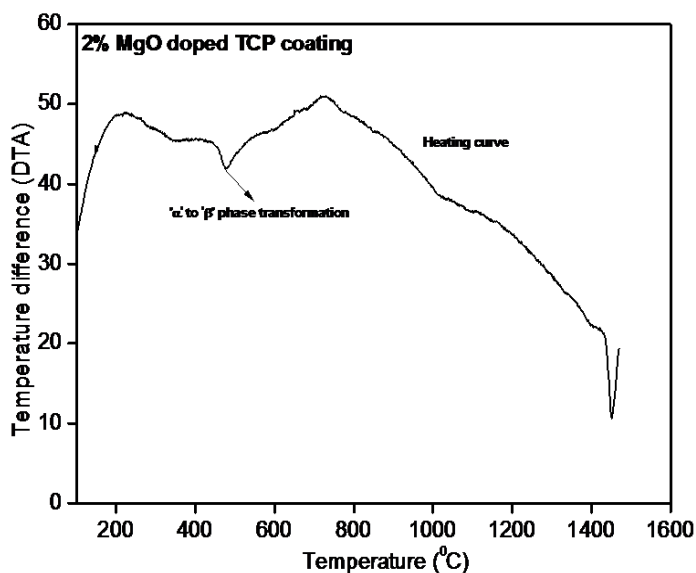


Figure 34: DTA spectrum of plasma sprayed samples

From the XRD and DTA spectra, the temperature range in between 700 and 800°C shows the complete phase transformation temperature of α to β TCP. Ti surface shows some kind of oxidation process above 850°C. [71–73] So the temperature has to be fixed at 800°C to obtain TCP coatings without α phase. Based on this inference all other coatings were heat treated at this temperature for removing the unwanted phase like α .

<i>Powder</i>	<i>Temperature (°C)</i>	<i>HA</i>	<i>βTCP</i>	<i>αTCP</i>
A	600	10.5	48.7	40.8
	700	12.1	84.1	3.8
	800	14.2	85.8	0
B	600	15.5	43.3	41.2
	700	14.4	81.1	4.04
	800	16.9	83.1	0
C	600	67.7	16.7	15.7
	700	70.4	27.9	1.7
	800	72.0	28	0

Table 13: Percentage of phase transformation of α to β with temperature obtained from MAUD analysis

Table 13 shows the phase compositions of each phase obtained after successful thermal treatment of CaP based coatings. It explains that at

800°C, α phase was completely removed and HA and β TCP was obtained. In powders A and B, 14 and 16% HA phases are obtained respectively. In powder C, HA phase is 72% and β TCP phase is 28%.

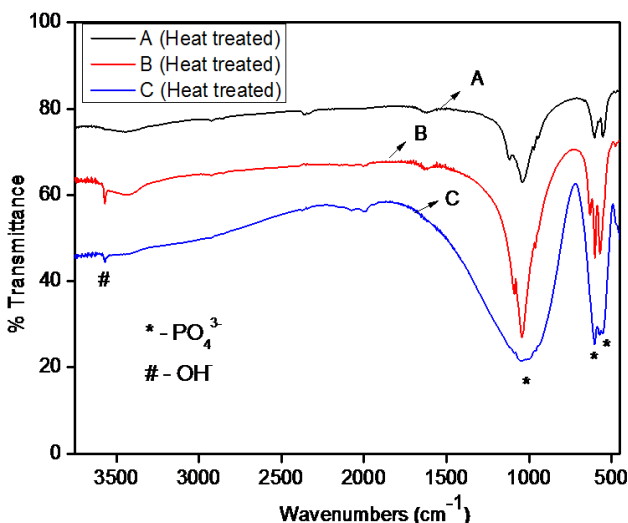


Figure 35: FT-IR spectrum of coatings after thermal treatment at 800°C

In the IR spectrum (*figure 35*), after the thermal treatment β TCP peaks reappeared at 1115, 980 and 960 cm^{-1} in samples 'A' and 'B'. These vibrations confirm the formation of β TCP during thermal treatment. The OH vibrational peaks of HA is observed at 3561 and 3563 cm^{-1} in samples 'B' and 'C'. The vibrations observed at 464, 552 and 608 cm^{-1} corresponds to the PO_4^{3-} groups present in the considered samples.

The SEM images of the sample cross section after thermal treatment (**figure 36-38**) reveal that, the coatings do not show any change compared with initial coatings. Samples are uniform in nature and are in good contact with Ti surface after thermal treatment also. The average coating thickness of the coatings is $\sim 80 - 90 \mu\text{m}$.

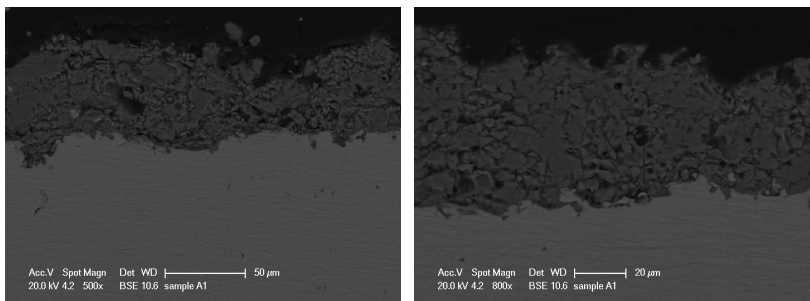


Figure 36: Cross section images of sample 'A' coated on Ti surface after thermal treatment.

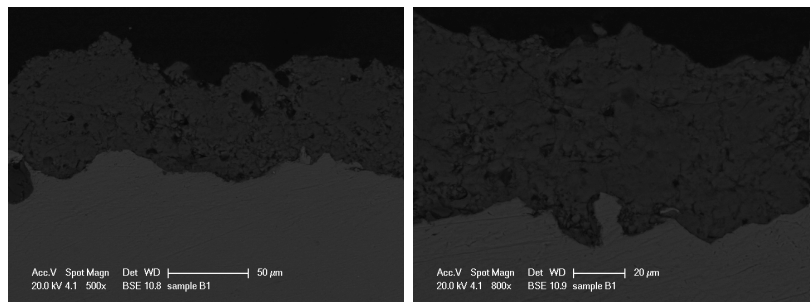


Figure 37: Cross section images of sample 'B' coated on Ti surface after thermal treatment.

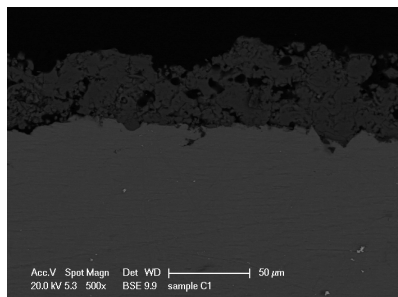
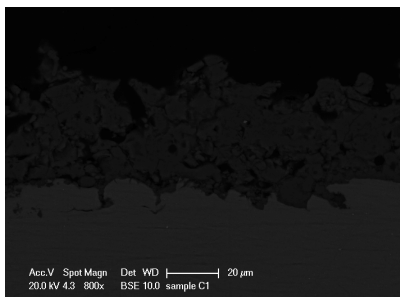


Figure 38: Cross section images of sample 'C' coated on Ti surface after thermal treatment

The β TCP and HA/ β TCP coatings were successfully fabricated using plasma spray and successful thermal treatment.

3.1.8. Invitro studies of TCP coatings

3.1.9. Bioactivity behaviour

The bioactivity behaviour (leaching) of the plasma sprayed coatings were analysed using simulated body fluid for 28 days at 37°C. After the studies the samples were investigated by SEM.

Figures 39-41, shows the cross sectional SEM images of considered sample after the leaching studies in SBF solution for 28 days. The images shows, the outer most leached HA layer of approximately 30-40 μm thicknesses for all the samples and shows some cracking perpendicular to the interface indicating mechanical weakening due to leaching. The Ca/P ratio of the HA top coat has 1.37 for sample 'A', 1.38 for 'B' and 1.46 for 'C'. *Kurzweg et al* reported about the new HA top coat formation during the leaching studies of plasma sprayed HA.[4]

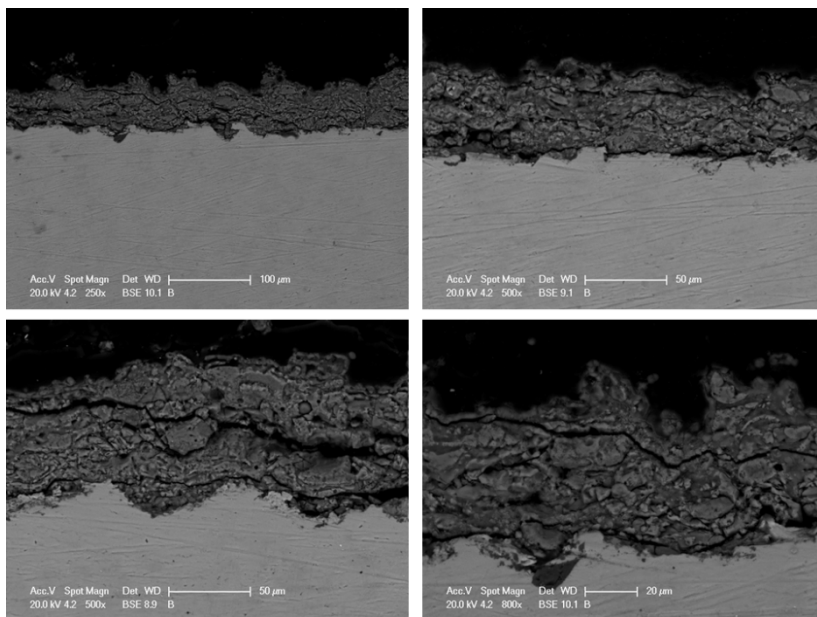


Figure 39: SEM images of sample 'A' after 28 days leaching process

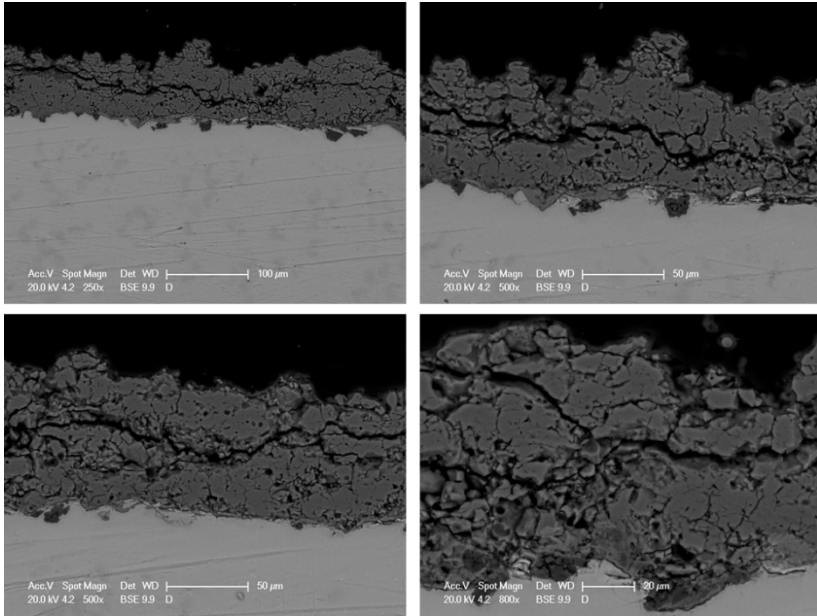


Figure 40: SEM images of sample 'B' after 28 days leaching process

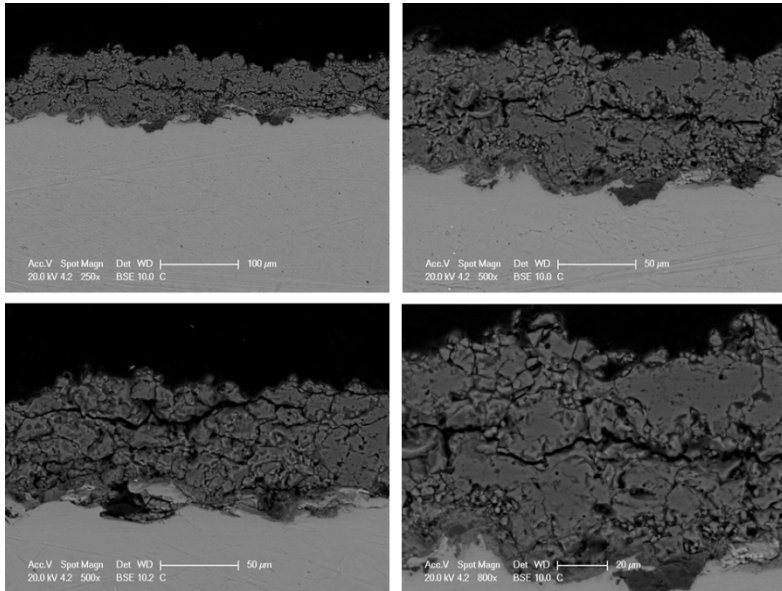


Figure 41: SEM images of sample 'C' after 28 days leaching process

3.1.10. Solubility measurements

The solubility measurements were carried out for 24 days in pH 5.5 MES buffer solution. Every 4 day the concentration of Ca/P was analysed using ICP. **Figure 42** shows the solubility trends of considered samples. Sample 'D', represents the conventional HA coating, which obtained from Eurocoating spa, Italy. This we used for a comparative study with our newly prepared calcium phosphate coatings.

The Ca and P concentrations obtained from ICP analysis are plotted against time.

Figure 42 shows the Ca and P concentration during measurement period. The dissolution of the samples is completely depends on the chemical compositions and surface morphology of the coatings.

In terms of dissolution of Ca and P, the order of solubility of most common calcium phosphate materials are: TTCP>> α TCP>> β TCP>> HA. [74]

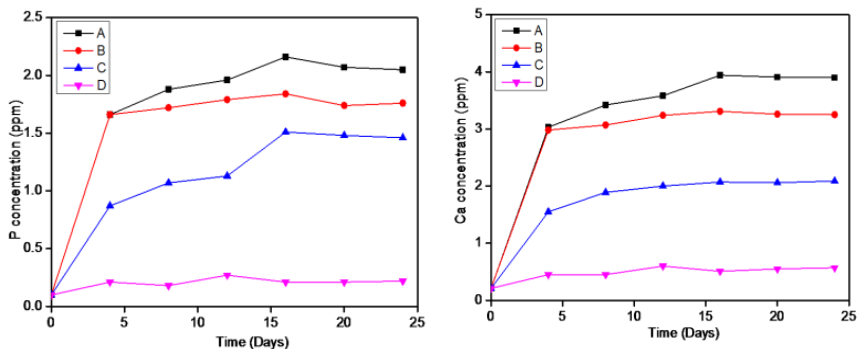


Figure 42: Ca and P concentrations versus time: MES buffer solution at pH 5.5

In our studies, samples are following the same trend. Sample 'A' shows more solubility rate compared with 'B'. This is mainly due to the presence of higher amount of MgO in sample 'B'. The Sample 'C' shows the solubility rate higher than that of conventional HA coatings (sample D). From this observation the HA/ β TCP shows better solubility rate than conventional HA coatings. [75][76]

For the concentration product calculation same methods are used for all the samples, is due to the fact that, it is not possible to calculate the Ksp value of biphasic compounds. Sample A and B contains >10% of HA phase and it consider as biphasic calcium phosphate. Ksp depends on the particular formula of specific monophasic compound.

The results obtained after calculating the concentration product values are reported in **Table 14**.

Sample	Ca/P ratio	Concentration product $[Ca^{2+}]^{10}[PO_4^{3-}]^6$
A	1.45	1.95×10^{15}
B	1.47	1.13×10^{14}
C	1.53	4.3×10^{11}
D	1.64	0.6×10^2

Table 14: Concentration product of coatings in MES solution

Plasma sprayed β TCP and HA/ β TCP coatings were successfully fabricated using plasma spray method and thermal process. The coatings show good biological performance. The newly produced plasma sprayed coatings also obtained leached HA top coat formation in SBF solution after 28 days. The solubility studies reveals that the presence of β TCP increases the dissolution rates of HA and the HA/ β TCP is more soluble than HA in MES buffer solution. The solubility behaviour of calcium phosphates in MES buffer solution is, TTCP>> α TCP>> β TCP>> HA/ β TCP>> HA.

Chapter 4: Conclusion

In the present work, β TCP and HA/ β TCP coatings were successfully fabricated using plasma spray and successive thermal treatments.

The β TCP and HA/ β TCP powders were synthesized using solid state method and MgO is used as a phase stabilizer. The synthesized powders were characterized using XRD, SEM, TG/DTA, ICP etc. The obtained powders were granulated and used for the plasma spray coating process. After the coating process the β phase of TCP is transformed to α phase. For analysing the stability of obtained α phase, the coatings were subjected to the thermal treatment at 500-1100°C for 15 min. - 2h. At 800°C, the ' α ' phase present in the plasma sprayed calcium phosphate coating is completely transformed to β phase and β TCP and HA/ β TCP coatings are obtained. The successively produced coatings were characterized and the Invitro properties like solubility and bioactivity behaviours are measured. The bioactivity properties were analysed by soaking the plasma spray coated samples in SBF at 37°C for 1 – 4 weeks. After 4 weeks, new leached HA top coat layer with average thickness 30 – 40 μ m was observed in the surface of the coatings.

The solubility measurement was analysed with MES buffer solution for 24 days. The solubility behaviour of calcium phosphates in MES buffer solution is, TTCP>> α TCP>> β TCP>> HA/ β TCP>> HA.

Therefore the β TCP and HA/ β TCP coatings were soluble faster than HA and slower than α TCP. The newly fabricated β TCP and HA/ β TCP plasma sprayed coatings showed better biological performance in SBF and MES buffer solution.

Reference:

- [1] Tathe A, Ghodke M, Nikalje A. A brief review: biomaterials and their application. *Int J Pharm Pharm Sci* 2010;2:19–23.
- [2] Patel N, Gohil P. A review on biomaterials: scope, applications & human anatomy significance. *Int J Emerg Technol Adv Eng* 2012;2:91–101.
- [3] Hung K-Y, Lo S-C, Shih C-S, Yang Y-C, Feng H-P, Lin Y-C. Titanium surface modified by hydroxyapatite coating for dental implants. *Surf Coatings Technol* 2013;231:337–45.
- [4] Kurzweg H, Heimann RB, Troczynski T, Wayman ML. Development of plasma-sprayed bioceramic coatings with bond coats based on titania and zirconia. *Biomaterials* 1998;19:1507–11.
- [5] Hench LL. Bioceramics: From Concept to Clinic. *J Am Ceram Soc* 1991;74:1487–510.
- [6] Thamaraiselvi T V, Rajeswari S. Biological Evaluation of Bioceramic Materials - A Review 2004;18:9–17.
- [7] Kannan S, Goetz-Neunhoeffler F, Neubauer J, Ferreira JMF. Ionic substitutions in biphasic hydroxyapatite and β -tricalcium phosphate mixtures: Structural analysis by rietveld refinement. *J Am Ceram Soc* 2008;91:1–12.
- [8] N. Rangavittal, A. R. Landa, J. M. González-Calbet, M. Vallet-Regí. Structural study and stability of hydroxyapatite and β -tricalcium phosphate : Two important bioceramics. *J Biomed Mater Res*; 51, 660–668, 2000

-
- [9] Mohandes F, Salavati-Niasari M. Influence of morphology on the in vitro bioactivity of hydroxyapatite nanostructures prepared by precipitation method. *New J Chem* 2014;38:4501.
- [10] Predoi D, Vatasescu-balcan RA, Pasuk I, Trusca R, Costache M. Calcium phosphate ceramics for biomedical applications 2008;10:2151–5.
- [11] Epple M, Ganesan K, Heumann R, Klesing J, Kovtun a., Neumann S, et al. Application of calcium phosphate nanoparticles in biomedicine. *J Mater Chem* 2010;20:18.
- [12] Shepherd JH, Shepherd D V, Best SM. Substituted hydroxyapatites for bone repair. *J Mater Sci Mater Med* 2012;23:2335–47.
- [13] Salimi MN, Bridson RH, Grover LM, Leeke G a. Effect of processing conditions on the formation of hydroxyapatite nanoparticles. *Powder Technol* 2012;218:109–18.
- [14] Jarcho M, Bolen CH, Thomas MB, Bobick J, Kay JF, Doremus RH. Hydroxylapatite synthesis and characterization in dense polycrystalline form. *J Mater Sci* 1976;11:2027–35.
- [15] Stewart M, Welter JF, Goldberg VM. Effect of hydroxyapatite/tricalcium-phosphate coating on osseointegration of plasma-sprayed titanium alloy implants. *J Biomed Mater Res A* 2004;69:1–10.
- [16] Li Y, Li Q, Zhu S, Luo E, Li J, Feng G, et al. The effect of strontium-substituted hydroxyapatite coating on implant fixation in ovariectomized rats. *Biomaterials* 2010;31:9006–14.

-
- [17] Surmenev R a, Surmeneva M a, Ivanova A a. Significance of calcium phosphate coatings for the enhancement of new bone osteogenesis--a review. *Acta Biomater* 2014;10:557–79.
- [18] Roy M, Bandyopadhyay A, Bose S. Induction plasma sprayed Sr and Mg doped nano hydroxyapatite coatings on Ti for bone implant. *J Biomed Mater Res B Appl Biomater* 2011;99:258–65.
- [19] Zhou X, Siman R, Lu L, Mohanty P. Argon atmospheric plasma sprayed hydroxyapatite/Ti composite coating for biomedical applications. *Surf Coatings Technol* 2012;207:343–9.
- [20] Klein CP, Patka P, van der Lubbe HB, Wolke JG, de Groot K. Plasma-sprayed coatings of tetracalciumphosphate, hydroxyl-apatite, and alpha-TCP on titanium alloy: an interface study. *J Biomed Mater Res* 1991;25:53–65.
- [21] Piccinini M, Rebaudi A, Sglavo VM, Bucciotti F, Pierfrancesco R. A new HA/TTCP material for bone augmentation: an in vivo histological pilot study in primates sinus grafting. *Implant Dent* 2013;22:83–90.
- [22] Roy M, Bose S. Osteoclastogenesis and osteoclastic resorption of tricalcium phosphate: effect of strontium and magnesium doping. *J Biomed Mater Res A* 2012;100:2450–61.
- [23] Ryu H, Youn H, Sun K, Chang B. An improvement in sintering property of b-tricalcium phosphate by addition of calcium pyrophosphate 2002;23:909–14.
- [24] Ryu H-S, Hong KS, Lee J-K, Kim DJ, Lee JH, Chang B-S, et al. Magnesia-doped HA/ β -TCP ceramics and evaluation of their biocompatibility. *Biomaterials* 2004;25:393–401.

-
- [25] Carrodeguas RG, De Aza AH, Turrillas X, Pena P, De Aza S. New Approach to the $\beta \rightarrow \alpha$ Polymorphic Transformation in Magnesium-Substituted Tricalcium Phosphate and its Practical Implications. *J Am Ceram Soc* 2008;91:1281–6.
- [26] Banerjee SS, Tarafder S, Davies NM, Bandyopadhyay A, Bose S. Understanding the influence of MgO and SrO binary doping on the mechanical and biological properties of beta-TCP ceramics. *Acta Biomater* 2010;6:4167–74.
- [27] Hesaraki S, Farhangdoust S, Ahmadi K, Nemati R, Khorami M. Phase evaluation and lattice parameters of strontium / magnesium incorporated beta-tricalcium phosphate bioceramics 2012;48:166–72.
- [28] Bose S, Tarafder S, Banerjee SS, Davies NM, Bandyopadhyay A. Understanding in vivo response and mechanical property variation in MgO, SrO and SiO₂ doped β -TCP. *Bone* 2011;48:1282–90.
- [29] Pan Y. Preparation of β -TCP with high thermal stability by solid reaction route 2003;8:1049–56.
- [30] Kien PT, Maruta M, Tsuru K, Matsuya S. Effect of phosphate solution on setting reaction of α -TCP spheres 2010;46:8–11.
- [31] Cüneyt Taş a, Korkusuz F, Timuçin M, Akkaş N. An investigation of the chemical synthesis and high-temperature sintering behaviour of calcium hydroxyapatite (HA) and tricalcium phosphate (TCP) bioceramics. *J Mater Sci Mater Med* 1997;8:91–6.
- [32] Enderle R, Götz-Neunhoeffler F, Göbbels M, Müller F a, Greil P. Influence of magnesium doping on the phase transformation

-
- temperature of beta-TCP ceramics examined by Rietveld refinement. *Biomaterials* 2005;26:3379–84.
- [33] Sasidharan Pillai R, Sglavo VM. Effect of MgO addition on solid state synthesis and thermal behavior of beta-tricalcium phosphate. *Ceram Int* 2015;41:2512–8.
- [34] Mayer I, Cuisinier FJG, Gdalya S, Popov I. TEM study of the morphology of Mn²⁺-doped calcium hydroxyapatite and beta-tricalcium phosphate. *J Inorg Biochem* 2008;102:311–7.
- [35] Matsumoto N, Sato K, Yoshida K, Hashimoto K, Toda Y. Preparation and characterization of beta-tricalcium phosphate co-doped with monovalent and divalent antibacterial metal ions. *Acta Biomater* 2009;5:3157–64.
- [36] Xue W, Dahlquist K, Banerjee A, Bandyopadhyay A, Bose S. Synthesis and characterization of tricalcium phosphate with Zn and Mg based dopants. *J Mater Sci Mater Med* 2008;19:2669–77.
- [37] Bandyopadhyay A, Bernard S, Xue W, Bose S. Calcium Phosphate-Based Resorbable Ceramics: Influence of MgO, ZnO, and SiO₂ Dopants. *J Am Ceram Soc* 2006;89:2675–88.
- [38] Kannan S, Ventura JM, Ferreira JMF. Aqueous precipitation method for the formation of Mg-stabilized β -tricalcium phosphate: An X-ray diffraction study. *Ceram Int* 2007;33:637–41.
- [39] Kannan S, Lemos IAF, Rocha JHG, Ferreira JMF. Synthesis and characterization of magnesium substituted biphasic mixtures of controlled hydroxyapatite / β -tricalcium phosphate ratios 2005;178:3190–6.

-
- [40] Kannan S, Goetz-Neunhoeffler F, Neubauer J, Pina S, Torres PMC, Ferreira JMF. Synthesis and structural characterization of strontium- and magnesium-co-substituted beta-tricalcium phosphate. *Acta Biomater* 2010;6:571–6.
- [41] Araújo JC, Sader MS, Moreira EL, Moraes VC a., LeGeros RZ, Soares G a. Maximum substitution of magnesium for calcium sites in Mg- β -TCP structure determined by X-ray powder diffraction with the Rietveld refinement. *Mater Chem Phys* 2009;118:337–40.
- [42] Ando J. Tricalcium Phosphate and its Variation By Jumpei ANDO (Received 1957;31:196–201.
- [43] Kitsugi T, Nakamura T, Oka M, Senaha Y, Goto T, Shibuya T. Bone-bonding behavior of plasma-sprayed coatings of BioglassR, AW-glass ceramic, and tricalcium phosphate on titanium alloy. *J Biomed Mater Res* 1996;30:261–9.
- [44] Liu X, Chu PK, Ding C. Surface modification of titanium, titanium alloys, and related materials for biomedical applications. *Mater Sci Eng R Reports* 2004;47:49–121.
- [45] Lugscheider E, Weber T. Plasma spraying--An innovative coating technique: Process variants and applications. *IEEE Trans Plasma Sci* 1990;18:968–73.
- [46] Singh G, Singh H, Sidhu BS. Characterization and corrosion resistance of plasma sprayed HA and HA-SiO₂ coatings on Ti-6Al-4V. *Surf Coatings Technol* 2013;228:242–7.
- [47] Heimann RB, Graßmann O, Jennissen HP, Zumbink T. Biomimetic processes during in vitro leaching of plasma-sprayed hydroxyapatite

coatings for endoprosthetic applications. *Materwiss Werksttech* 2001;32:913–21.

- [48] Gomes PS, Botelho C, Lopes M a, Santos JD, Fernandes MH. Evaluation of human osteoblastic cell response to plasma-sprayed silicon-substituted hydroxyapatite coatings over titanium substrates. *J Biomed Mater Res B Appl Biomater* 2010;94:337–46.
- [49] Yang C, Lui T. Effect of Hydrothermal Self-Healing and Intermediate Strengthening Layers on Adhesion Reinforcement of Plasma-Sprayed Hydroxyapatite Coatings. 2004;10.
- [50] Cheang P, Khor K a. Addressing processing problems associated with plasma spraying of hydroxyapatite coatings. *Biomaterials* 1996;17:537–44.
- [51] Dey A, Nandi SK, Kundu B, Kumar C, Mukherjee P, Roy S, et al. Evaluation of hydroxyapatite and β -tri calcium phosphate microplasma spray coated pin intra-medullary for bone repair in a rabbit model. *Ceram Int* 2011;37:1377–91.
- [52] Tsui YC, Doyle C, Clyne TW. Plasma sprayed hydroxyapatite coatings on titanium substrates Part 2 : optimisation of coating properties 1998;19.
- [53] Lugovskoy A, Lugovskoy S. Production of hydroxyapatite layers on the plasma electrolytically oxidized surface of titanium alloys. *Mater Sci Eng C* 2014;43:527–32.
- [54] Heimann RB. Design of Novel Plasma Sprayed Hydroxyapatite-Bond Coat Bioceramic Systems 1999;8:597–603.

-
- [55] Prev y PS. X-RAY DIFFRACTION CHARACTERIZATION OF CRYSTALLINITY AND PHASE COMPOSITION IN PLASMA-SPRAYED HYDROXYLAPATITE COATINGS 2000;9:369–76.
- [56] Fielding GA, Roy M, Bandyopadhyay A, Bose S. Acta Biomaterialia Antibacterial and biological characteristics of silver containing and strontium doped plasma sprayed hydroxyapatite coatings. Acta Biomater 2012;8:3144–52.
- [57] Song Y-G, Cho I-H. Characteristics and osteogenic effect of zirconia porous scaffold coated with β -TCP/HA. J Adv Prosthodont 2014;6:285–94.
- [58] Ryu H-S, Hong K-S, Lee J-K, Kim DJ, Lee JH, Chang B-S, et al. Magnesia-doped HA/beta-TCP ceramics and evaluation of their biocompatibility. Biomaterials 2004;25:393–401.
- [59] Daculsi G, Passuti N, Martin S, Deudon C, Legeros RZ, Raher S. Macroporous calcium phosphate ceramic for long bone surgery in humans and dogs. Clinical and histological study. J Biomed Mater Res 1990;24:379–96.
- [60] Nery EB, LeGeros RZ, Lynch KL, Lee K. Tissue response to biphasic calcium phosphate ceramic with different ratios of HA/beta TCP in periodontal osseous defects. J Periodontol 1992;63:729–35.
- [61] Gauthier O, Bouler JM, Aguado E, Pilet P, Daculsi G. Macroporous biphasic calcium phosphate ceramics: Influence of macropore diameter and macroporosity percentage on bone ingrowth. Biomaterials 1998;19:133–9.
- [62] Daculsi G, LeGeros RZ, Nery E, Lynch K, Kerebel B. Transformation of biphasic calcium phosphate ceramics in vivo: ultrastructural and

physicochemical characterization. J Biomed Mater Res 1989;23:883–94.

- [63] Matsumoto N, Yoshida K, Hashimoto K, Toda Y. Preparation of Beta-Tricalcium Phosphate Powder Substituted with Na/Mg Ions by Polymerized Complex Method. J Am Ceram Soc 2010;93:3663–70.
- [64] Mahesh K V., Anas S, Rahul S, Ananthakumar S. Effect of two-step sintering on rare earth (RE = Y₂O₃, Pr₆O₁₁) doped ZnO–Bi₂O₃ varistors processed from “nano-precursor” powders. J Mater Sci Mater Electron 2012.
- [65] Sasidharan Pillai Rahul , K. V. Mahesh, S. S. Sujith, Mathews Jeen Maria . J Electroceramics 2014;32:292–300
- [66] Rahul SP, Mahesh K V., Sujith SS, Jeen Maria M, Ananthakumar S. Processing of La₂O₃ based rare earth non-linear resistors via combustion synthesis. J Electroceramics 2014;32:292–300.
- [67] Oyane A, Kim H-M, Furuya T, Kokubo T, Miyazaki T, Nakamura T. Preparation and assessment of revised simulated body fluids. J Biomed Mater Res A 2003;65:188–95.
- [68] DeVoe K, Banerjee S, Roy M, Bandyopadhyay A, Bose S. Resorbable Tricalcium Phosphates for Bone Tissue Engineering: Influence of SrO Doping. J Am Ceram Soc 2012;95:3095–102.
- [69] Berzina-Cimdina L, Borodajenko N. Research of Calcium Phosphates Using Fourier Transform Infrared Spectroscopy. Infrared Spectrosc – Mater Sci Eng Technol 2012:123–48.

-
- [70] Meejoo S, Maneepprakorn W, Winotai P. Phase and thermal stability of nanocrystalline hydroxyapatite prepared via microwave heating. *Thermochim Acta* 2006;447:115–20.
- [71] Matveev V a, Pleshanov NK, Bulkin a P, Syromyatnikov VG. The study of the oxidation of thin Ti films by neutron reflectometry. *J Phys Conf Ser* 2012;340:012086.
- [72] Jamesh M, Sankara Narayanan TSN, Chu PK. Thermal oxidation of titanium: Evaluation of corrosion resistance as a function of cooling rate. *Mater Chem Phys* 2013;138:565–72.
- [73] Gemelli E, Camargo NH a. Oxidation kinetics of commercially pure titanium. *Matéria (Rio Janeiro)* 2007;12:525–31.
- [74] Kannan S, Goetz-Neunhoeffler F, Neubauer J, Ferreira JMF. Synthesis and structure refinement of zinc-doped β -tricalcium phosphate powders. *J Am Ceram Soc* 2009;92:1592–5.
- [75] Moreno EC, Gregory TM, Brown WE. Preparation and solubility of hydroxyapatite. *J Res Natl Bur Stand Sect A Phys Chem* 1968;72A:773.
- [76] Li X, Ito A, Sogo Y, Wang X, Legeros RZ. Solubility of Mg-containing b-tricalcium phosphate at 25 ° C 2009;5:508–17.
- [77] LeGeros RZ. Calcium phosphate-based osteoinductive materials. *Chem Rev* 2008;108:4742–53.
- [78] Barradas AMC, Yuan H, van Blitterswijk C a., Habibovic P. Osteoinductive biomaterials: current knowledge of properties, experimental models and biological mechanisms. *Eur Cell Mater* 2011;21:407–29.

-
- [79] Dorozhkin S. Medical Application of Calcium Orthophosphate Bioceramics. *Bio* 2011;1:1–51.
- [80] Boanini E, Gazzano M, Bigi a. Ionic substitutions in calcium phosphates synthesized at low temperature. *Acta Biomater* 2010;6:1882–94.
- [81] Silver F. H. and Ch. Doillon; *Biocompatibility. Interaction of Biological and Implantable Materials*; VCH Publisher Inc., New York (1989)

Acknowledgements

I would like to thank my parents Sasidharan Pillai and Prasanna Kumari, my wife Vani, my sister Saranya, brother in law Renjith and all other family members for their heartfelt support and encouragement during my entire life to achieve my dreams.

Sincere thanks to Prof. V M Sglavo for his continuous support during my PhD programme. His patience, constant motivation and encouragement had helped me to make progress in my research career. His guidance helped me in all the time of PhD programme including writing of this thesis.

Thanks to Prof. S. Dire for her valuable advices during my entire PhD programme.

Thanks to Eurocoating S.p.A for plasma spray process and financial funding.

I would like to thank Dr. K.G.K Warriar and Dr. S. Ananthakumar for offering me a chance to work as a part of their research group in NIIST-CSIR India.

Thanks to Livio, Alexia and Lorena for helping me to analyse the samples.

I would like to express my sincere thanks to my friends especially, Rony, Pradeep, Aravind, Tinku, Sajna, Shine, Shaji, Sajid, Meera, Mahesh, Linsha, George, Krishnan, Lekshmi kanth, Rahul and so on for helping me to finish my dream.

Finally I would like to thanks my colleagues Kiran, Anshu, Pradnyesh, Lam, Ali, Vincenzo, Mattia, Matteo, Daniele, Francesca and so on for the kind support.

Without the help and assistance from all these special people this thesis would not have been completed.

Curriculum Vitae

Educational Background

PhD: Department of Industrial Engineering, University of Trento, Trento, Italy (2012 - 2015)

Dissertation: ***"Synthesis and Characterization of Calcium Phosphate Powders for Biomedical Applications by Plasma Spray Coating"***

MSc.: General Chemistry, University of Kerala, Thiruvananthapuram, India (2007-2009)

Thesis: ***"Effects of Chemicals in Waste Paper Deinking"***

BSc.: General Chemistry, University of Kerala, Thiruvananthapuram, India (2004-2007)

Research Experience

Junior Research Fellow: Material science department, NIIST-CSIR, Thiruvananthapuram, Kerala, India (2010 – 2012).

Project fellow: R & D department, Hindustan Newsprint Ltd. Kottayam, Kerala, India (March 2009 – June 2009)

Publications

- 1) F. Munarin, P. Petrini, P.F. Robotti, **R.S. Pillai**, S. Dirè, M.C. Tanzi, V.M. Sglavo, "Micro- and Nano- Hydroxyapatite as Active Reinforcement for Soft Biocomposites". *Int. J. Biol. Macromol.* 72 (2014) 199-209.
- 2) **Rahul Sasidharan Pillai**, Vincenzo M. Sglavo, "Effect of MgO incorporation and synthesis temperature on phase stability of beta tricalciumphosphate". *Ceramic international*, 41, (2015), 2512-2518.
- 3) **Sasidharan Pillai Rahul**, K.V. Mahesh, S. Sujith, Jeen M and S. Ananthakumar, "Processing of La₂O₃ based Rare Earth Non-Linear Resistors via Combustion Synthesis". *J. Electroceramics*, 32, (2014), 292-300.
- 4) K.V. Mahesh, S. Anas, **S. Rahul**, and S. Ananthakumar, "Effect of two-step sintering on rare earth (RE- Y₂O₃, Pr₆O₁₁) doped ZnO-Bi₂O₃ varistors processed from, 'nano- precursor' powders". *J. mater. Sci: Mater.Electron*, 24 (2013) 1495-1504.
- 5) Anas Shereef, **Rahul Sasidharan**, Babitha K B, Mangalraja R Viswanathan and S. Ananthakumar, "Microwave Accelerated Synthesis of UV and Visible Light Active ZnO Nanoplates".(*Arabian J. chem.*, Under review)

-
- 6) Jeen M, **Sasidharan Pillai Rahul**, K.V. Mahesh, S. Sujith, and S. Ananthakumar, "Effect of silica doping on rare Earth Non-Linear Resistors through gel Combustion method". (*J. Am. Ceram. Soc.*, Under review)
 - 7) **Rahul Sasidharan Pillai**, Vincenzo M. Sglavo, "βTCP and HA/βTCP plasma sprayed coatings for implant applications". (Manuscript under preparation).

Conferences

- 1) **R. Sasidharan Pillai** and V.M. Sglavo, "Effect of MgO Incorporation and Synthesis Temperature on Phase Stability of Beta Tricalciumphosphate", Oral poster presentation, Euromate-2014, Lausanne, Switzerland, July 21- 25, 2014.
- 2) **Sasidharan Pillai Rahul**, John down, S. Dirè, V.M. Sglavo. "Mg incorporation into beta tricalciumphosphate (β TCP) powder for high temperature phase stability", Oral communication, ICACC-2014, Dyatona beach, Florida, USA. January 24 -29, 2014.
- 3) **Sasidharan Pillai Rahul**, S. Dirè, V.M. Sglavo, "Synthesis and Characterization of Phase Stabilized HA/ β TCP Composite Powder", Oral communication, Summer school on Biomaterials and Regenerative Medicine, Riva Del Garda, Italy, July 08th – 12th , 2013
- 4) F. Munarin, P. Petrini, S. Dirè, M.C. Tanzi, P.F. Robotti, **R S. Pillai**, V.M. Sglavo. "Injectable nano HA particles-containing pectin composite gels", Oral communication, Nanotechnologies for Health Care, Trento, May 25th -26th, 2012.
- 5) **Rahul S**, Mahesh K.V, Ananthakumar S. "Solar thermal control ZnO/SiO₂ ceramic- polymer hybrid coatings for energy efficient

buildings”, Oral communication, 73rd Indian Ceramic Society Conference, December 19th-22nd, 2011

- 6) **Rahul S**, Mahesh K.V, Ananthakumar S. “Rare-earth oxide varistors for surge-protection application”, Poster communication, Rare Earth International Conference (STAR -2011), August-2011.

Thank you